DEVELOPMENT OF FIBER OPTIC PROBES AND A DUAL WAVELENGTH LASER SYSTEM FOR MEDICAL APPLICATIONS

A THESIS SUBMITTED TO

THE GRADUATE SCHOOL OF ENGINEERING AND SCIENCE

OF BILKENT UNIVERSITY

IN PARTIAL FULFILLMENT OF THE REQUIREMENTS FOR

THE DEGREE OF

MASTER OF SCIENCE

IN

MATERIAL SCIENCE AND NANOTECHNOLOGY

By

Elif Uzcengiz Şimşek

January 2016

DEVELOPMENT OF FIBER OPTIC PROBES AND A DUAL WAVELENGTH LASER SYSTEM FOR MEDICAL APPLICATIONS

By Elif Uzcengiz Şimşek

January 2016

We certify that we have read this thesis and that in our opinion it is fully adequate, in scope and in quality, as a thesis for the degree of Master of Science.

Bülend Ortaç(Advisor)

Süleyman Serdar Kozat

Selçuk Aktürk

Approved for the Graduate School of Engineering and Science:

Levent Onural
Director of the Graduate School

ABSTRACT

DEVELOPMENT OF FIBER OPTIC PROBES AND A DUAL WAVELENGTH LASER SYSTEM FOR MEDICAL APPLICATIONS

Elif Uzcengiz Şimşek
M.S. in Material Science and Nanotechnology
Advisor: Bülend Ortaç
January 2016

Optical fibers have been widely used in the past several decades due to their characteristics, such as laser energy transmission, low optical loss and different beam shape. These features make them advantegous for different applications in a number of fields such as telecommunication, imaging, laser cavity systems and medical applications. Fiber optic probes were developed to use optical fiber systems in medicine since they are flexible, small in diameter, easy to use and they transmit the laser energy through the target tissue of the body without any additional optical alignment. The tip geometry of the fiber optic probes can be changed so that the laser radiation is emitted with different shapes. Flat-ended, side-firing, radial, double radial and diffusing fiber optic probes, having different beam shapes, were developed by using mechanical polishing and also, CO_2 laser polishing technique was demonstrated for fining radial fiber tips for the first time throughout this study. The probes were analyzed in terms of ray tracing, Zemax modelling, fabrication and light deflection. As a result, the spatial distribution of the fabricated probes were optimized. Different beam shapes originating from each fiber optic probe can serve for specific purposes. One of them is to use the diffusing probe as a cladding light stripper (CLS) in the fiber laser cavity since it improves the beam quality of the fiber laser. On the other hand, endovenous laser ablation (EVLA) is one of the operations that flat, radial and double radial probes are preferred for ablating the varicose vein reflux, which is a common disease seen in 25% of women and 15% of men in the USA. A dual-wavelength medical laser system (980nm-1470nm), operating both at continuous wave (cw) and pulsed wave (pw), was also developed and characterized in terms of spectrum, power and pulse duration. A whole medical laser system consisting of the home-made radial fiber optic probe and the dual-wavelength medical laser system was assembled. In conclusion, design, development and characterization of the fiber optic probes having different beam shapes were performed and two different applications, namely CLS and a dual-wavelength medical laser system, were presented.

Keywords: Fiber optic probes, cladding light strippers, dual wavelength medical laser system, endovenous laser ablation (EVLA).

ÖZET

MEDİKAL UYGULAMALAR İÇİN FİBER OPTİK PROBLAR VE İKİLİ DALGA BOYLU LAZER SİSTEMİ GELİŞTİRİLMESİ

Elif Uzcengiz Şimşek
Material Science and Nanotechnology, Yüksek Lisans
Tez Danışmanı: Bülend Ortaç
Aralık 2015

Optik fiberler, lazer enerjisini doğrusal olmayan bir şekilde taşıyabilmeleri, düşük optik kayıp ve ışığı farklı şekillerde yayabilmeleri gibi özellikleri dolayısıyla yaygın bir şekilde kullanılmaktadır. Bu avantajlı özelliklerinden dolayı telekomunikasyon, görüntüleme, lazer rezenatör sistemleri ve medikal uygulamalarda tercih edilmektedir. Optik fiberler, esnek bir yapıya sahip olmaları, çaplarının küçük olması, lazer enerjisini vücut içerisinde bulunan hedef dokulara rahatlıkla ulaştırabilmeleri dolayısıyla tıbbì uygulamalarda kullanılmaktadır. Ayrıca, uç geometrileri değiştirilerek, lazer enerjisinin dağılımı farklı şekillerde elde edilebilir. Bu çalışmada, düz-uç, yan-atım, radyal, çiftli radyal ve dağıtıcı uçlu optik problar mekanik zmparalama ve CO_2 lazer cilalama teknikleri ile gelitirilmişdir. Geliştirilen problar, ışın teorisi, Zemax analizleri, üretilme teknikleri ve ışık dağılım ölçümleri ile incelenmiştir. Böylece, fiberlerin uzaysal dağılım profilleri optimize edilmiştir. Farklı uç geometrisine sahip her bir fiber prob için farklı bir uygulama alanı vardır. Dağıtıcı fiber uçlarının, fiber lazer sistemlerinde kılıf ışığı sıyırıcısı olarak kullanılması bu alanlardan biridir. Kılıfta ilerleyen ışık, kılıf ışığı sıyırıcı tarafından çıkarılarak lazer ışık kalitesi yükseltilmiş olur. Diğer bir taraftan, düz uç, radyal ve çiftli radyal uçlu problar yaygın bir hastalık olan varis tedavisinde, diğer bir deyişle, endövenöz lazer ablasyonunda (EVLA) kullanılırlar. ABD'de kadınların %25'i ve erkeklerin %15'i bu hastalğa yakalanmaktadırlar. EVLA operasyonunda kullanılmak üzere, ikili dalga boyunda, hem sürekli hem de atımlı dalga boyunda çalşabilen bir lazer sistemi tasarlanmş; spektrum, güç ve atım özellikleri karakterize edilmiştir. Varis tedavisinde kullanılmak üzere hem radyal fiber probu hem de ikili dalga boylu lazer sistemi bir araya getirilmiştir. Sonuç olarak, farklı uzaysal dağılıma sahip fiber optik problar tasarlanmış, geliştirilmiş ve karakterize edilmiştir ve iki farklı alan olan kılıf ışığı sıyırıcı

olarak fiber lazer sisteminde; fiber prob olarak ikili dalga boyuna sahip bir medikal lazer sisteminde kullanılmıştır.

Anahtar sözcükler: Fiber optik problar, kılıf ışığı sıyırıcı, ikili dalgaboylu medikal lazer sistemi, endovenöz lazer ablasyon (EVLA).

Acknowledgement

I acknowledge that apart from my effort, the encouragement and guideness of many other people contributed to the success and existence of this study. Firstly, I would like to express my sincere gratitude to my advisor Assist. Prof. Dr. Bülend Ortaç for giving me this opportunity and his endless help, support, encouragement, guideness, and supervision for this study. I also would like to thank Dr. Erol Özgür and Ali Aytaç Seymen for giving me this opportunity to be a part of this project and their endless help.

This work is partially supported by TUBITAK under the project number of 113A055. I acknowledge support from Turkish Academy of Sciences under the TUBA-GEBİP program and Bilim Akademisi - The Science Academy Turkey under the BAGEP program. This work is partially supported by TUBITAK under the 1501 program, project number 3140846. I would like to express my sincere gratitude to TUBITAK for their support.

I would like to thank to our research group members for their friendship, encouragement and support. I would like to thank Canan Kurşungöz who was there for me to complete this thesis with her encouragement, support, patience, positive attitude and lovely friendship and also thank Dr. Tolga Bağcı for helping and encouraging me for this work. I would like to thank Yakup Midilli for helping and guiding me for the experimental procedure in the lab. I would like to thank to Bartu Şimşek as my husband, friend, group member, diving-body and the one who always cheers me up for his help for experimental work, encourage, love, and especially his deep patience. I also thank to Refik Tuzaklı for his friendship and encouregement. I want to thank to new member of our research group O. Benjamin Efunbajo for his friendship. I would like to thank to Yağmur Yılmaz, who is R&D engineer at EA Teknoloji, for her endless help for the laboratory work and her contributions to our research. My special thank goes to our laboratory technician Levent Ersoy who always helps me to set experimental setup and his friendship.

I would like to thank to UNAM members, friends and staff for their support and friendship. I want to thank to Gamze Torunoğlu for her help for the AFM study.

I would like to thank to my family, my father Orhan Uzcengiz, who passed away eight years ago, my lovely mother Şükran Uzcengiz, my lovely sister Yasemin Orak and her husband Alican Orak, my mother in-law Leyla Şimşek, my father in-law Özer Şimşek and my little sweety sister in-law Tuana Şimşek for their endless love, encourage and support.

Contents

List of Figures

Chapter 1

Introduction

In the past several decades, optical fibers have attracted a great attention since they transmit laser energy, with low-loss and with different beam shape [1]. They are especially used in several fields such as telecommunication, imaging, laser cavity systems and medical applications. In this thesis, medical application of fiber optic probes will be studied. Fiber optic probes are widely used in the clinical environment due to their various advantages. They are flexible, small in diameter, easy to use since they can transmit laser energy through the target tissue in the body without any additional optical alignment. Fiber optic probes emit laser radiation with different shapes by changing their tip geometry [2]. Flat-ended, side-firing, radial, double radial and diffusing fiber probes have different beam shapes which are specific to a medical application. Flat-ended, radial and double radial probes are widely used in endovenous laser ablation (EVLA) [3]. Side-firing probes are used in prostate [4], breast cancer tumor ablation [5]. Diffusing fiber probes are preferred for photodynamic theraphy [6]. The fiber optical probe consists of three main parts, namely optical connector, fiber and its tip. One of them is optical connector and the other part is tip geometry. An optical connector is a tool that provides that fiber plug in and out of the laser without optical alignment [7]. Fiber optical probes are easy to use, fast and user friendly thanks to optical connector. Besides the optical connector, fiber tip geometry is the significant part of the fiber optic probes since laser energy can be emitted with different shapes by changing the fiber tip geometry. Therefore, laser energy can be transmitted through the target tissue in the body with a preferred beam shape and position. The probes that mentioned above will be investigated in terms of ray tracing analysis, Zemax modelling, fabrication and light deflection characterization. In the fabrication part, two types of polishing techniques were used. One of them is mechanical polishing which is performed by polishing machine and lapping (polishing) films. This process is a time-consuming process and laborer dependent. Therefore, CO_2 laser polishing, which is the second technique, will be explained and was demonstrated in radial fiber probes after forming the fiber tip geometry by mechanical polishing for the first time. Also, a new approach of fabricating double ring radial fiber optic probe will be investigated.

The rest of this thesis includes development of a dual wavelength medical laser system mainly used for EVLA. The medical laser is working at two different wavelengths, 980nm and 1470nm, respectively. 980nm is mostly used in EVLA, however, in the recent studied it is reported that longer wavelengths are much more efficient. In order to build the medical laser system, dual wavelength diode was analyzed in terms of spectra, wavelength shift with the change in cooling temperature, power and power stability. This analysis was used to build a feedback supported cooling system. The medical laser system can operate in both continuous wave (cw) and pulsed wave (pw) modes. Pulsed mode is provided by electronical circuit. Interval, duration, power, number of pulses, operating wavelength and mode (cw or pw) can be selected in the user interface.

Chapter 2

Theory of Light Guiding in a Cylindrical Waveguide

Fiber Optics - Historical Background

Guiding light in a long narrow material has been studied for recent decades. After invention of lasers in 1960, transmitting information in a long distances using light became a great opportunity [8]. Light can carry the information faster than microwaves due to high optical frequencies [9]. After invention of the ruby-laser, using fiber optics for long-distance communication is stand out. Thus, the enormous development on the fiber optic technology has begun and still continues today [10] . The main principle of guiding light in a dielectric media is total internal reflection (TIR) with spesific conditions. The silica glass surrounded by air is used as a cylindrical waveguide. However, glass-air interface which is non-homogeneous and has discontinuous points lead to high optical loss [11]. The decibel (dB) is a logarithmic unit that implies a ratio between a level of quantity to reference. In fiber optics, dB unit is generally used for expressing the laser power. In 1966, Kao and Hockham have published an important paper stating that the necessary transimission medium conditions can be provided by silica glass based an optical fiber structure, thus, metallic and other impurities would

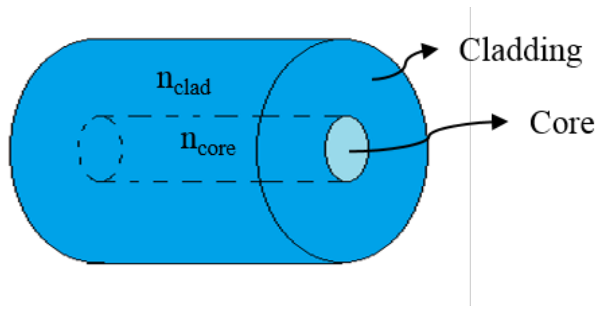

Figure 2.1: Schematic drawing of an optical fiber.

be eliminated. The scheme of the optical fiber structure which is composed of an inner cylinder glass core having refractive index n_{core} and an outer cylinder glass having refractive index $n_{cladding}$ slightly smaller than n_{core} is represented in figure 2.1. Also, they predicted that the attenuation should be around $20dB/km$ [12]. In 1966, the same group have obtained $1000dB/km$ experimentally even when the most transparent and perfect glass was used. $1000dB/km$ means that the optical power could be transmitted only with 20 meter-long optical fiber. Clearly, this optical power loss value is too large to use optical fibers in communication even for the short distances. In 1970, Kapron, Keck and Maurer (at Corning Glass) have achieved $17dB/km$ with He-Ne laser having wavelength $633nm$ of by producing silica fibers [13]. $17dB/km$ means that an optical signal could be transmitted inside the fiber $40km$ with $0.25dB/km$ loss [14]. This breakthrough opens a door for applications of optical fibers at many markets such as high energy application, biomedical and clinical applications, smart structures, security, military, and process control [15].

2.1 Ray Tracing Theory and Fundamental Concepts

An optical fiber usually has cylindrical symmetrical geometry. Ray tracing method is an easy and useful technique which covers almost all the characteristics of the travelling light inside an optical fiber. It is applied in two-dimensions. The fundamental concepts used in two-dimensional ray tracing are Snell law, critical angle, total internal reflection, numerical aperture and acceptence angle. These concepts are related with each other, but all of them represent a different feature of optical fiber [16]. These concepts are explained in the following chapter.

2.1.1 Snell's Law

Light coupled inside a fiber travels by reflecting from the boundary of core and cladding. In order to understand the light guiding inside an optical fiber, refractive index, which is the basic feature of the core and cladding, should be examined. Refractive index for a medium can be explained as proportion of velocity of light in vacuum and velocity of light in that medium. Light moves slower inside a denser medium (larger refractive index) and moves faster inside a less dense medium (smaller refractive index) [17]. This phenomenon can be clarified by Snell Law in equation 2.1 .

$$n_1 \sin\theta_1 = n_2 \sin\theta_2 \tag{2.1}$$

2.1.2 Critical Angle

Critical angle is a special case when incoming ray travels along the boundary between two media having different refractive index values. When $\theta_1 < \theta_{critical}$, the incoming ray is partially reflected from the boundary and refracted through the next medium, as represented in figure 2.2.b. In figure 2.2.c, critical angle condition is represented when $n_1 > n_2$. Incoming ray could not pass through the next medium when θ_2 becomes $\frac{\pi}{2}$ and θ_1 becomes critical angle ($\theta_{critical}$) [18]. The refractive index of the medium that ray is coming from must be greater than the refractive index of the next medium. The critical angle can be extracted from the equation 2.2 below:

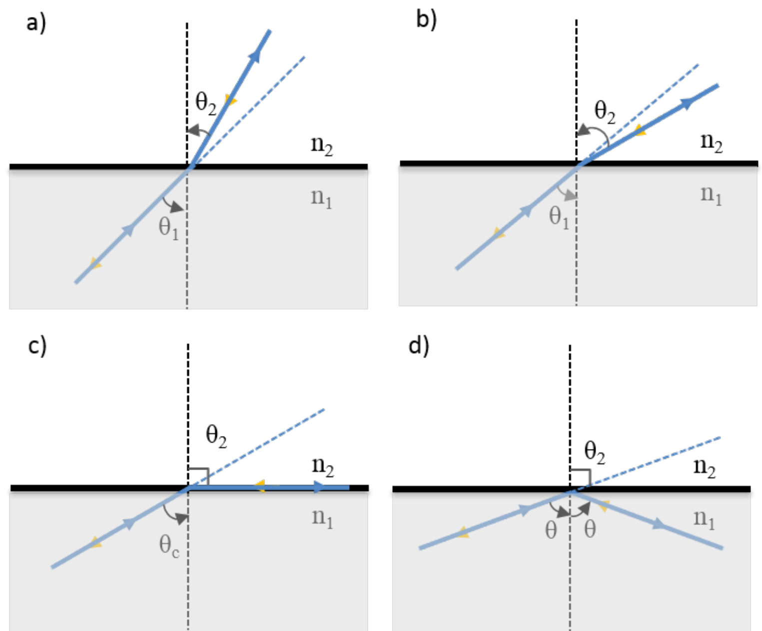

Figure 2.2: Snell Law. The cases are a) $n_1 < n_2$, b)$n_1 > n_2$, c) θ_c : critical angle when ,$n_1 > n_2$, d) total internal reflection (TIR), $n_1 > n_2$ and $\theta > \theta_c$.

$$\theta_c = \arcsin(\frac{n_2}{n_1}) \tag{2.2}$$

For instance, the critical angle between air and glass can be found as 41.8° since refractive index of the air is 1 and that of the glass is 1.5 by using equation 2.2.

$$\theta_c = \arcsin(\frac{1}{1.5}) = 41.8° \tag{2.3}$$

2.1.3 Total Internal Reflection

Total internal reflection is a special case when propagating ray hits to a boundary between two media having different refractive indices, and it is reflected totally from that point without any refraction since the angle between the surface and the normal is larger than the critical angle for that boundary [19]. When θ_1 is greater than the θ_c, all the incoming rays begin to reflect from the boundary, none of them passes through the next medium and travel through the medium where they are coming from. This is called as total internal reflection (TIR). The total internal reflection is shown in the figure 2.2.d. This phenomenon is the fundamental case for fiber optics. Optical fibers are cylindirical wave guides that allow the light waves propagating with a low loss. The waves coupled inside an optical fiber travel by confirming the TIR. The signal loss due to reflection and refraction is minimized since the geometry of the optical fibers and refractive index distribution inside the optical fiber are set in order to confirm TIR. In figure 2.3, an optical fiber is represented. The rays are travelling inside the fiber with totally reflecting from the core and cladding boundary. The rays prefer to propagate inside the core due to refractive index distribution and coupling angle to the fiber. The coupling is another important issue for fiber optics. It will be explained in the following two subsections.

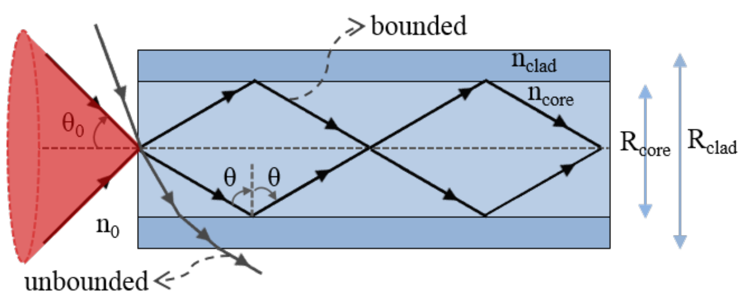

Figure 2.3: Total internal reflection (TIR) inside an optical fiber. The case for refractive index of media: $n_{core}>n_{clad}>n_0$, the case for reflection angles is $\theta>\theta_c$. n_0 is refractive index of air, θ_0 is acceptance angle, R_{core} is diameter of the core, and R_{clad} is the diameter of the cladding

2.1.4 Numerical Aperture

An optical fiber can be considered as a cylindrical dielectic waveguide which is composed of two concentric glass cylinders. One of them is core having refractive index n_{core}, the other one is cladding having refractive index n_{clad}. In order to ensure total internal reflection (figure 2.3) inside the fiber, n_{core} should be greater than n_{clad}. The medium outside can be considered as air having refractive index, $n_\circ$, smaller than both n_{core} and n_{clad}. These refractive index values form the coupling conditions for an optical fiber. Every optical fiber has a numerical aperture (NA) which is one of the feature that implies the coupling condition inside the fiber [20]. Numerical aperture depends on refractive indices mentioned above, n_{core}, n_{clad} and $n_\circ$. The formula is for NA can be written as:

$$NA = \sqrt{n_{core}^2 - n_{clad}^2} \tag{2.4}$$

For instance, the numerical aperture value of the fiber having $n_{core} = 1.4501$ and $n_{cladding} = 1.3923$ can be calculated as using equation 2.4:

$$NA = \sqrt{1.4501^2 - 1.3923^2} = 0.40 \tag{2.5}$$

2.1.5 Acceptance Angle

The angle which is the maximum boundary for allowing TIR and providing the light coupling inside the optical fiber is called as acceptance angle. The acceptance angle is represented in figure 2.3. This angle is also refered as half-cone angle (in 3D). If the incoming ray angle with fiber end-face normal is smaller than the acceptance angle, the ray couples into the fiber and travels with TIR. These kinds of rays are called as bounded modes. If the angle between fiber end-face normal is greater than acceptance angle, the ray could not couple into the fiber and TIR cannot occur inside the fiber. Then, the ray is refracted from the cladding to air or evanesce in the cladding. These kinds of rays are called as unbounded modes. If we write the acceptance angle condition to the equation 2.1:

$$n_\circ \sin\theta_\circ = n_{core}\sin(90 - \theta_{critical}) \tag{2.6}$$

When $\cos\theta_c$=$\sin(90 - \theta_c)$, it becomes $\cos\theta_c$=$\sqrt{1 - \sin^2\theta_{critical}}$. Also, using equation 2.2, the acceptance angle becomes:

$$\theta_\circ = \arcsin(\frac{NA}{n_\circ}) \tag{2.7}$$

For instance, acceptance angle of the fiber having numerical aperture 0.40 can be calaculated using equation 2.7, in the air medium which assumed to have refractive index value as 1:

$$\theta_\circ = \arcsin(\frac{0.40}{1}) = 23.57^\circ \tag{2.8}$$

2.1.6 Brewster Angle

Brewster angle is such a condition that the polarization of the light get importance. At Brewster angle, the reflection coefficient becomes zero for p-polarized light when the polarization is parallel to the normal of plane. There is no such angle confirming this condition for s-polarized light [21]. Therefore, the reflected light becomes p-polarized when unpolarized light hit the boundary. The illustration for this condition can be considered as figure 2.2.a or b. For this case, reflection and transmission coefficients are important. Reflection and transmission coefficients can be written as following and the Brewster angle is calculated among them [22]:

$$r_{p-polarized} = \frac{n_1 \cos\theta_2 - n_2 \cos\theta_1}{n_1 \cos\theta_2 + n_2 \cos\theta_1} \tag{2.9}$$

$$t_{p-polarized} = \frac{2n_{1\cos\theta_1}}{n_2 \cos\theta_1 + n_1 \cos\theta_2} \tag{2.10}$$

$$r_{s-polarized} = \frac{n_1 \cos\theta_1 - n_2 \cos\theta_2}{n_1 \cos\theta_1 + n_2 \cos\theta_2} \tag{2.11}$$

$$t_{s-polarized} = \frac{2n_{1\cos\theta_1}}{n_1 \cos\theta_1 + n_2 \cos\theta_2} \tag{2.12}$$

When $n_1 \cos\theta_2 = n_2 \cos\theta_1$, $r_{p-polarized}$ becomes zero and using equation 2.1:

$$n_1^2 \cos^2 \theta_2 = n_2^2 \cos^2 \theta_1 \tag{2.13}$$

Using trigonometrical formula:

$$\frac{n_2^2}{n_1^2} \cos^2 \theta_1 = 1 - \frac{n_1^2}{n_2^2} \sin^2 \theta_1 \tag{2.14}$$

Since $\cos x = \frac{1}{\sec x}$, the equation becomes:

$$\frac{n_2^2}{n_1^2} = \sec^2 \theta_1 - \frac{n_1^2}{n_2^2} \tan^2 \theta_1 = 1 + (1 - \frac{n_1^2}{n_2^2}) \tan^2 \theta_1 \tag{2.15}$$

And, the θ_1 becomes Brewster angle, θ_B :

$$\theta_B = \arctan \frac{n_2}{n_1} \tag{2.16}$$

The Brewster angle between air ($n_\circ = 1$) and glass ($n_{glass} = 1.45$) can be calculated as:

$$\theta_B = \arctan \frac{1}{1.45} = 34.59^\circ \tag{2.17}$$

2.1.7 Multi Mode and Single Mode Fibers

The rays enter the fiber if it is in the limit of acceptance angle and then, they travel inside the optical fiber. They follow a path inside the fiber core where the rays are travelling. These paths are called as modes inside an optical fiber. If the core of the fiber is large enough, rays have many paths to travel, and the fiber is called as a multimode fiber. If the core of the fiber allows only one path to travel, then fiber is called as single mode. The illustration is represented in figure 2.4:

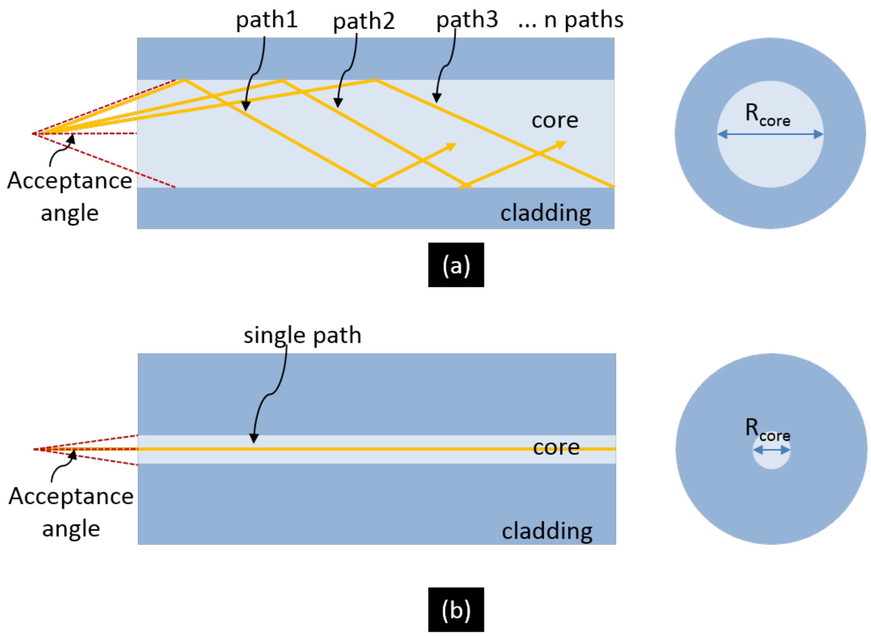

Figure 2.4: Illustration of (a) multimode and (b) single mode fibers

The radii of the core and the cladding give an idea about the mode-distribution inside the fiber. For multimode fibers, the R_{core} is approximately $50\mu m$ or larger. For single mode fibers, R_{core} has a value between $2-10\mu m$ [23].

2.2 Electromagnetic Theory for Optical Radiation

The light is an electromagnetic wave. In order to explain light travelling inside an optical fiber, electromagnetic theory is used. Maxwell equations explain the mathematics of the wave-like behaviour of the light [24]. The electromagnetic waves are investigated to understand wave-like nature of the light inside a cylindrical dielectic medium, which is optical fiber.

2.2.1 Electromagnetical Waves

Maxwell equations are written as below equations 2.18 to 2.21 [25]. $\vec{E}$ is electric field, $\vec{H}$ is magnetic field, $\vec{D}$ is electric flux density, and $\vec{B}$ is magnetic flux density and ρ_V is electric volume charge density. In equation 2.18 [25],

$$\nabla \times \vec{E} = -\frac{\partial \vec{B}}{\partial t} \tag{2.18}$$

$$\nabla \times \vec{H} = -\frac{\partial \vec{D}}{\partial t} \tag{2.19}$$

$$\nabla \cdot \vec{D} = \rho_v \tag{2.20}$$

$$\nabla \cdot \vec{B} = 0 \tag{2.21}$$

when,

$$\vec{D} = \varepsilon \vec{E}, and \vec{B} = \mu \vec{H} \tag{2.22}$$

Taking curl of $\nabla \times \vec{E}$ and $\nabla \times \vec{H}$, we get:

$$\nabla \times (\nabla \times \vec{E}) = -\mu\varepsilon \frac{\partial^2 \vec{E}}{\partial^2 t} \tag{2.23}$$

$$\nabla \times (\nabla \times \vec{H}) = -\mu\varepsilon \frac{\partial^2 \vec{H}}{\partial^2 t} \tag{2.24}$$

Using the identity $\nabla \times (\nabla \times \vec{A}) = \nabla(\nabla \cdot \vec{A})$ - $\nabla^2 \vec{A}$:

$$\nabla^2 \vec{E} = \mu\varepsilon \frac{\partial^2 \vec{E}}{\partial t^2} \tag{2.25}$$

$$\nabla^2 \vec{H} = \mu\varepsilon \frac{\partial^2 \vec{H}}{\partial t^2} \tag{2.26}$$

Scalar wave equation which is also known as Helmholtz equation:

$$\nabla^2 \Psi = \frac{1}{\upsilon_p^2} \frac{\partial^2 \Psi}{\partial t^2} \tag{2.27}$$

From below equation, we obtain velocity of light in that medium:

$$\upsilon_p = \frac{1}{\sqrt{\mu\varepsilon}} = \frac{1}{\sqrt{\mu_r \mu_0 \varepsilon_r \varepsilon_r}} \tag{2.28}$$

Ψ could be either $\vec{E}$ or $\vec{H}$. υ_p is the velocity of the light in that medium. Thus, it becomes the speed of light in vacuum.

$$c = \frac{1}{\sqrt{\mu_0 \varepsilon_0}} = 3 \times 10^8 \frac{m}{s} \tag{2.29}$$

For the cartesian coordinates left hand side of the equation 2.27 becomes:

$$\nabla^2 \Psi = \frac{\partial^2 \Psi}{\partial x^2} + \frac{\partial^2 \Psi}{\partial y^2} + \frac{\partial^2 \Psi}{\partial z^2} \tag{2.30}$$

Cylindrical coordinates for Helmholtz equation 2.27 becomes:

$$\nabla^2 \Psi = \frac{\partial^2 \Psi}{\partial r^2} + \frac{1}{r} \frac{\partial^2 \Psi}{\partial r^2} + \frac{1}{r^2} \frac{\partial^2 \Psi}{\partial \phi^2} + \frac{\partial^2 \Psi}{\partial z^2} + n^2 k_0^2 \Psi \tag{2.31}$$

The solution of the wave-equation is given as:

$$\Psi = \Psi_0 expi(\omega t - \vec{k} \cdot \vec{r}) \tag{2.32}$$

The equation 2.32 for three dimentional k becomes:

$$\Psi = \Psi_0 expi(\omega t - k_x t - k_y t - k_z t) \tag{2.33}$$

Where ω is angular frequency, t is time, $\vec{r}$ is the coordinate for measurement point and $\vec{k}$ is the propagation vector. $\vec{k}$ can be explained as below formula:

$$k = |\vec{k}| = \frac{2\pi}{\lambda} \tag{2.34}$$

where λ stands for wavelength of the light (wave).

2.2.2 Modes in Planar Waves

In order to ensure that light traveling inside core - cladding boundary with same phase after a few reflections, there are essential conditions. There are specific angles and bounded modes that allow the light propagation. These angles and modes can be specified with propagation constant, written in equation 2.35. [26]:

$$\beta_z = n_{core} k_0 \sin\theta = \frac{2\pi}{\lambda} \tag{2.35}$$

There are mainly three cases for β values, and they are explained as in the following:

case 1: $\frac{2\pi}{\lambda} n_{cladding} < \beta < \frac{2\pi}{\lambda} n_{core}$; The light travels inside the core obeying the TIR.

case 2: $\frac{2\pi}{\lambda} n_{coating} < \beta < \frac{2\pi}{\lambda} n_{cladding}$; The light travels inside cladding, totally reflected from cladding - coating boundary.

case 3: $\beta < \frac{2\pi}{\lambda} n_{coating}$; The light can not travel inside the fiber, it couples outside of the optical fiber.

2.2.3 Spatial Distribution of Modes in Cylindrical Waveguide

Helmholtz equation 2.27 is solved in order to indicate spatial distribution of the modes in a cylindrical waveguide (optical fiber). Using $\omega = 2\pi f$, Helmholtz equation (eqn. 2.27) can be written as following:

$$\nabla^2 \Psi = n^2 (k_0)^2 \Psi \tag{2.36}$$

The modes in propagating waves are in the direction of fiber, z-direction. Ψ is a periodic function since it represents a wave. Thus, Ψ can be written as periodic function with harmonic terms as $e^{-id\varphi}$, and the solution becomes:

$$\Psi(r, \varphi, z) = \Upsilon(\psi(r) e^{-id\varphi} e^{-i\beta z}) \tag{2.37}$$

In order to simplify these equations and eliminate the complex part, we can write equation 2.37 into equation 2.31, and we get differential equation for Bessel functions:

$$\frac{\partial^2 \psi}{\partial r^2} + \frac{1}{r}\frac{\partial \psi}{\partial r} + (n^2 k_0^2 - \beta^2 - \frac{d^2}{r^2})\psi = 0 \tag{2.38}$$

Modes that are coupled into the core should satisfy $n_{cladding} k_0 < \beta < n_{core} k_0$,

$$k_T^2 = n_{core}^2 k_0^2 - \beta^2 \tag{2.39}$$

and

$$\rho^2 = \beta^2 - n_{cladding}^2 k_0^2 \tag{2.40}$$

k_T is transverse wave number, and ρ is the decay parameter.

From equation 2.38. :

$$\frac{\partial^2\psi}{\partial r^2} + \frac{1}{r}\frac{\partial\psi}{\partial r} + (k_T^2 - \frac{d^2}{r^2})\psi = 0 \tag{2.41}$$

$$\frac{\partial^2\psi}{\partial r^2} + \frac{1}{r}\frac{\partial\psi}{\partial r} - (\rho^2 + \frac{d^2}{r^2})\psi = 0 \tag{2.42}$$

Equation 2.38 becomes equation 2.41 for core and equation 2.42 for cladding. These equations can be solved by Bessel functions when approaching infinity at $r \longrightarrow 0$ in the core and $r \longrightarrow \infty$ [27] .

2.3 Types of Fibers

Basic characteristics of the optical fibers are investigated in the previous sections. In this section, basic refractive index distributions of the optical fibers are studied. This distribution is an important characteristic for fibers [28]. Refractive index distribution affects the TIR and guiding inside the fiber. There are fibers having different refractive index distributions such as step-index, graded-index, panda mode, photonic crystal and so on [29]. In this section step-index and graded-index fibers are covered.

2.3.1 Step Index Fiber

In figure 2.5.a, a step-index fiber is illustrated. The refractive index distribution has a rectangular shape. Core and cladding boundary has a sharp difference in refractive index values. Rays are totally reflected from that boundary.

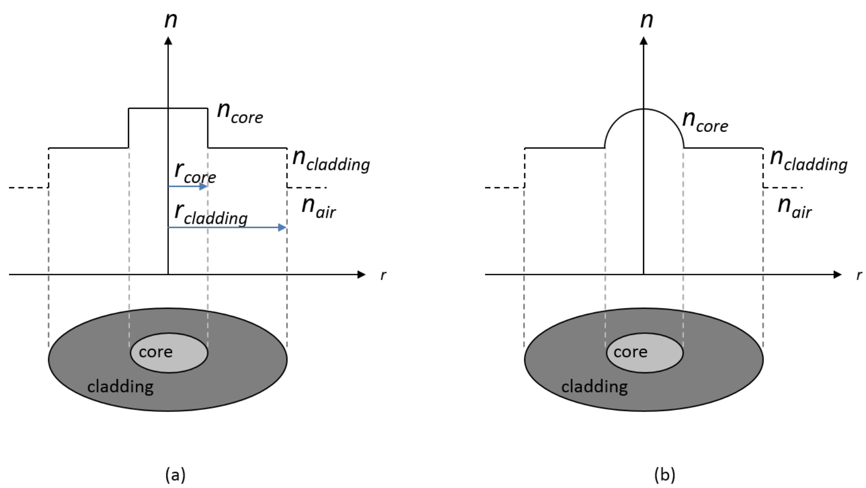

Figure 2.5: a)Step-index and b) graded-index fiber.

2.3.2 Graded Index Fiber

In figure 2.5.b, a graded index fiber is represented. The refractive index distirbution has semi-circle shape. There is no sharp boundary between core and cladding, therefore, the refractive index changes gradually from core to cladding. The rays are refracted gradually, they follow a bended-path and at some point between core and cladding, they are totally reflected. The graded-index fibers represent less mode-dispersion comparing to step-index fibers.

2.4 Losses in Optical Fibers

In the earlier developments, low-loss optical transmission was achieved with $\sim 0.2dB/km$ loss as mentioned in Chapter 2. There are three basic loss mechanisms in optical transmission in fibers namely scattering, absorption and bending loss. In figure 2.6, the loss mechanisms are represented. In the scattering case, a photon hits a boundary and changes its direction and photon may exit the fiber medium. The scattered photon continues to propagate outside the fiber. In the case of absorption, a photon propagating inside the fiber is absorbed by impurities or dopants, converted to energy and causes heat. The absorbed photon disappears inside the fiber. In the case of bending, the loss is independent from composition of the fiber (dopant, impurities), rather it occurs due to shape of the fiber. If the fiber is bended, the TIR could be violated, thus, the rays could not be reflected totally from the bended point, and they are partially reflected inside the fiber and refracted through the outside of the fiber [30].

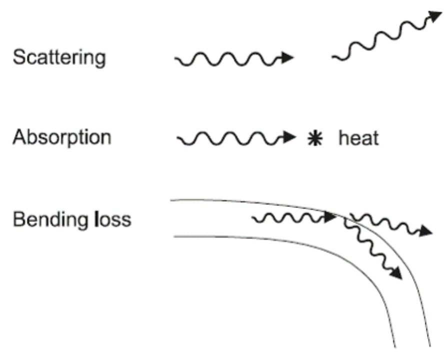

Figure 2.6: Three cases for power loss mechanism of optical fiber. (adapted from [30])

Chapter 3

Fiber Optic Probes

Fiber optic probes are quite useful tools for medical applications for treatment of diseased hollow organs [31]. They have a potential to improve clinical practice since the integration of fiber optic probes to medical lasers are used in the treatment of several diseases such as venous relux [32], breast [33] and prostate tumors [34]. Fiber optic cables are extensively prefered in the clinical environment due to their various advantages [35]. One of the advantage is that they could allow the laser beam to be transmitted non-linearly. Another advantage of fiber optic probe can be considered as the fiber optical connector which is the connection piece of the fiber with the laser device providing the fiber probes plug in and out without optical alignment [36]. Also, fibers can have various diameter values, ranging hundreds of microns to milimeters. Hence, it is easy to insert fibers into the diseased body parts due to their small diameters and they are used in minimally invasive laser theraphy. Minimally invasive applications provide a comfortable treatment period for patients [37]. It is safe to use, effective operational result and flexible structure. Fiber optical cables both transmit the laser energy to the targetted tissue and they deflect the laser energy with different emission shapes by manipulating their tip geometry [38]. It is possible to deflect the laser beam not only the same direction with the fiber but also side direction or radially. These fiber tip geometries are used for a specific medical application.

For example, flat-ended and radial fibers are used in Endovenous Laser Ablation (EVLA), side-firing probes are used in tumor ablation, diffusing probes are used in photodynamic theraphy [39]. In this chapter, development procedure of flat-ended, side-firing, radial emitting and diffusing fiber optical probes are discussed in terms of ray tracing analysis, modelling, fabrication and light deflection measurements. Their medical application fields are also mentioned. In the ray tracing analysis part, the rays were examined for flat, side-firing and radial tip geometries and the theories were used such as total internal reflection, Snells Law. After theoretical analysis, the ray tracing and light deflection were investigated by Zemax modelling. The fiber tip geometries were studied, and the fiber tip angles were determined, then the fiber optical probes were fabricated.

3.1 Designing a Fiber Optical System at Zemax

Zemax (Zemax,LLC, Germany) has been serving as an optical design software for 25 years and it has been used for developing, analyzing and improving optical systems such as imaging and illumination optics, lenses, mirrors and fibers [40]. The program models optical systems by using ray tracing. Rays come through the optical system and the program compiles the rays according to wavelength of the incoming rays, refractive index of the piece of the optical system, distance between optical parts of the system. Glass type is assigned by choosing the glass type from the library available in the software. The commercial lenses are also available in the library. There are three options to design an optical system: sequential, non-sequential and combination of sequential/non-sequential. In the sequential option, optical elements are analyzed by creating the optical system surface boundary by surface boundary. The rays are traced through the image plane and the features such as spot diagram, ray-fan plots can be analyzed. It is possible to give tolerance to the lenses due to manufacturing issues and optimize the lenses, and also fixing the aberations. In the non-sequential option, stray light and physical beam propagation can be analyzed. The geometry of the optical system can easily be created in the program by using non-sequential mode. There is another option, which is composed of both sequential and non-sequential.

This option combines the features of both. In our study, ray propagation inside the optical fiber and the fiber tip geometries were modelled. The best option is the non-sequential mode which is widely used for designing the optical fibers [41, 42]. Optical fiber propagation and the tip geometries were modelled in the non-sequential option and the deflection characteristics were analyzed.

3.2 Fabrication Procedure of Fiber Optic Probes

The first and crucial step for using fiber optic probes in medical applications is preparing the end-face of fiber optic precisely. The end-face of the optical fiber should be smooth in order to reduce the optical loss due to light scattering [43]. There are several optical fiber fining techniques such as hand polishing, mechanical polishing, acid etching and recently studied laser polishing procedures [44]. Fiber optical polishing is mainly starts with rough polishing to form the shape of the fiber tip. After the tip geometry is formed as flat, side-firing or conical, fine polishing is applied to complete the polishing procedure. Fine polishing is the crucial part since it is hard to polish the tip without deforming its shape. In this chapter, mechanical and laser polishing procedures are studied. Mechanical polishing is more widely used, however, it has some disadvantages such that it depends on the laborer, the time spent on polishing films is long. Laser polishing can be considered as a potential solution to disadvantages of mechanical polishing. However, the tip geometries cannot be formed by using only laser polishing, as will be explained in section 3.2.2. Therefore, the fiber tip geometries can be formed by rough mechanical polishing and fine polishing is applied by the laser radiation. Thus, process would be independent from laborer and takes less time [45].

3.2.1 Mechanical Fabrication Procedure

In order to form and fine the end-face of the fiber optic probe, mechanical polishing is widely used [46]. The process is basically rubbing the fiber end-face on the polishing films. The fiber is inserted inside the jig and the end-face of the fiber is pressed onto the films sticked on the disk. The films are changed according to their roughness, starting from rough to finer ones. Thus, the roughness of fiber end-face is also changed implicitly. There are commercially available polishing films: KrellTech (USA) and ThorLabs (USA). In our study, we used KrellTech polishing films and the roughness follows the order as $30\mu m$, $9\mu m$, $3\mu m$, $0.3\mu m$. In figure 3.1, KrellTech polishing films are shown. Flat-ended, side-firing, radial, double-ring radial and even diffuser fiber optical probes can be fabricated by using these films. Furthermore, the SEM images of KrellTech polishing films

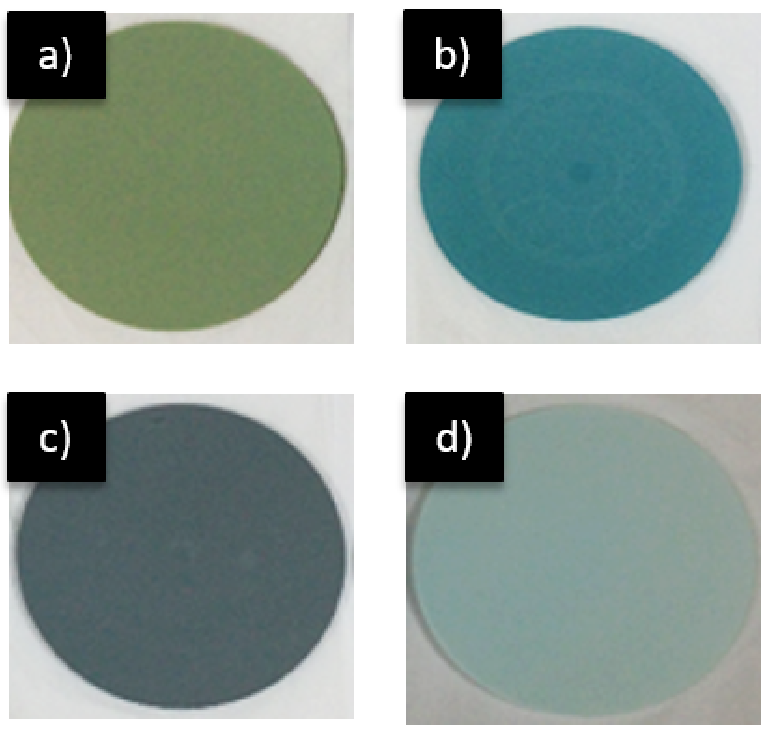

Figure 3.1: Polishing films having roughness a) 30 μm ,b) 9 μm ,c) 3 μm and d) 0.3 μm .

are shown in figure 3.2, and it is clearly seen that there are sharper and larger aluminum oxide particles in the rougher films. The particle sharpness and size are reduced which also allows decreasing the surface roughness of the film. These films are composed of alumina particles which are stronger materials than glass. Therefore, alumina particles located in the films can create abrasion on glass.

Polishing process is applied to the fiber which, has core/clad/coating diameters

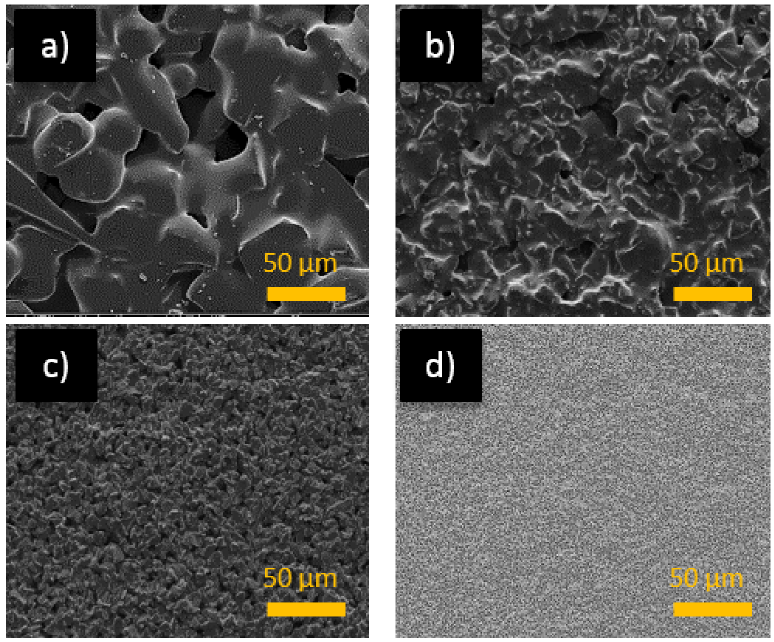

Figure 3.2: SEM images of polishing films having roughness a) 30 μm ,b) 9 μm ,c) 3 μm and d) 0.3 μm

as 400/425/730 micrometer. The core/clad/coating is composed of Silica/TECS (Hard Polymer Coating)/Tefzel buffers, respectively. The fiber's NA is 0.39 and it operates at 200-2200 nm low-OH fiber [ThorLabs, USA]. The fiber polisher is KrellTech-Trig Lite Fiber Polisher [USA]. In order to obtain flat-ended fiber tip, the fiber was positioned vertically (90°) to the polishing film.

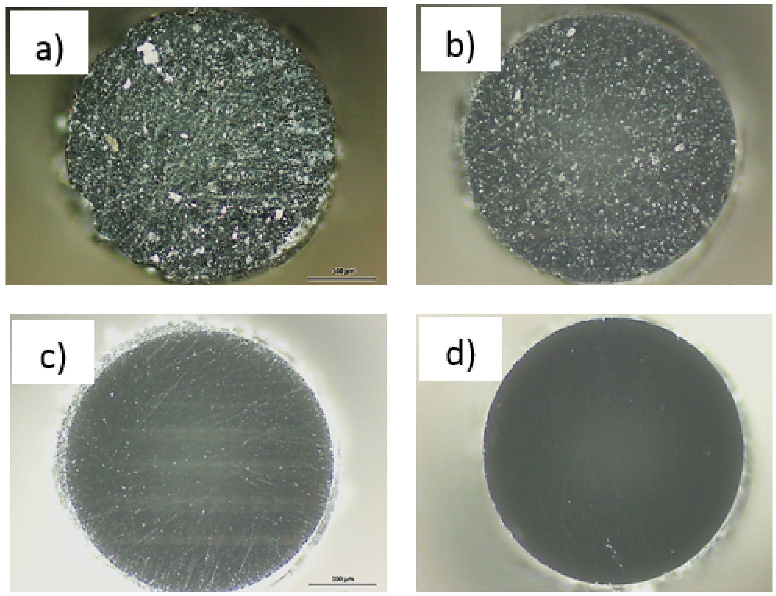

Figure 3.3: Optical microscope images of polished fiber end-faces having roughness a) 30 μm, b) 9 μm, c) 3 μm and d) 0.3 μm

In figure 3.3, polished fiber end-faces with different roughness are shown. Optical microscope images were taken in the dark field mode. The scratches, cracks and hitches can be seen clearly in the fiber end-face polished with 30μm polishing film in figure 3.3.a. In figure 3.3.b and c, the roughness slightly disapears and a smooth fiber end-face was achieved by using 0.3μm polishing film, and scattering losses became negligible shown in 3.3.d.

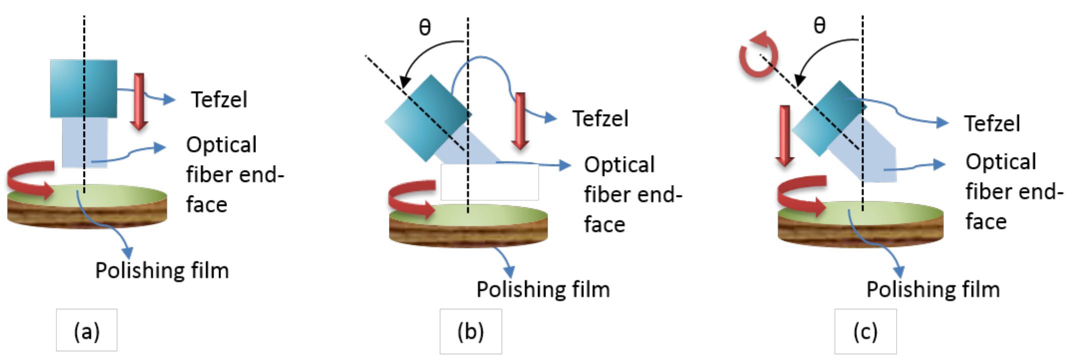

Figure 3.4: Polishing procedure for a) Flat-ended, b) side-firing, and d) radial fiber optical probe

As mentioned previously in this chapter, in order to use the fiber optical probes for medical applications, these polishing procedures should be applied first to flat-ended, side-firing and radial tip fibers. Side-firing and radial fiber probes are required to be positioned with an angle into the polishing machine as shown in the figure 3.4.b,c. Besides, in order to form conical shape, fiber rotates around its axis its center while polishing as represented in figure 3.4.c.

3.2.2 Laser Polishing Procedure

Laser polishing can be applied to the materials absorbing the radiation when $10.6\mu m$ CO_2 laser is exposed. The main principle of laser polishing is that thin layer of a material melts for a while and cools down after radiation [47]. The surface absorbing the radiation becomes smooth due to surface tension. In the silica-glass laser polishing process, low photon energy of the CO_2 laser ($0.2eV$) is not enough to brake Si-O bonds [48]. The laser radiation is absorbed by surface and this energy is converted to thermal energy. For silica-glass material, the absorption is very high in that regime, in the order of $10^3 cm^{-1}$ [49]. The laser radiation is absorbed by a thin layer with a very small penetration depth inside the material. The temperature of the silica does not reach the glass transition temperature when exposed to CO_2 laser since the energy is low [48]. Therefore, glass is not transferred to the liquid state, it stays at viscoelastic region. Using this effect as an advantage, the glass surface could be fined by $10.6\mu m$ CO_2 laser radiation [50]. The scattering and back reflection losses are minimized due to elimination of the imperfections existed after mechanical polishing. The laser

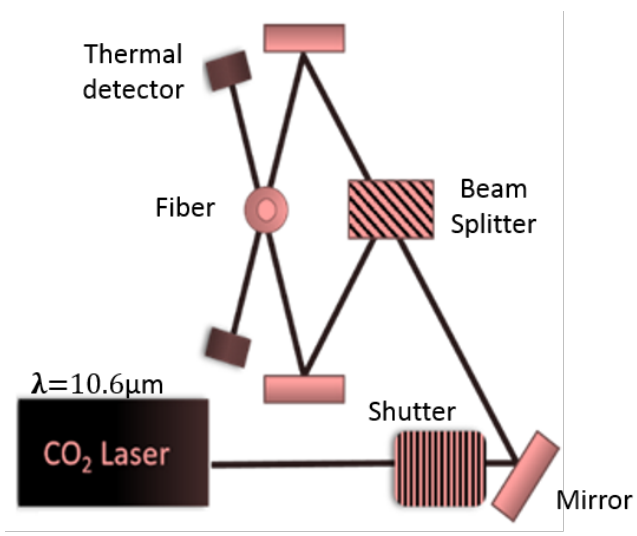

Figure 3.5: CO_2 laser polishing setup.

polishing setup used throughout the experiments of this study is shown in figure 3.5. The laser beam splits into two beams by beam splitter and is combined onto the fiber surface by mirrors. Thus, the fiber is exposed to the laser energy from both sides homogeneously. The shutter can be used as a chopper and it can transform continuous wave (cw) to pulsed wave (ps). The power of the CO_2 laser is measured by thermal detector. This scheme belongs to the LZM-100 LAZERMaster Laser Splicing System (AFL, USA). This device is usually used for tapering and splicing optical fibers using $10.6\mu m$ CO_2 laser radiation. Taking the advantage of writing special function which contains modulated laser energy (pulsed, chirped or continuous wave) into the device, the fiber end-face can be polished. The optical microscope images of laser-polished flat-ended fibers

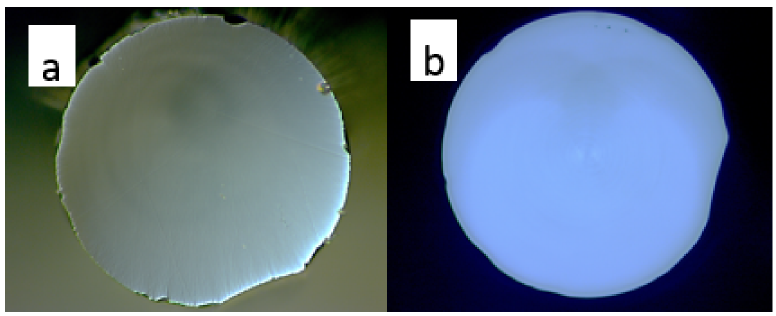

Figure 3.6: Optical microscope images of the same fiber end-face (a) fine mechanical and (b) after laser processed.

are shown in figure 3.6, the demonstration of laser polishing of flat-ended fiber is shown. The function written into the device is composed of 8 pulses of laser energy with 1s duration and 1s interval. Laser power density is $9.15x10^3 \frac{W}{cm^2}$. Figure 3.6.a belongs to fine-mechanically polished fiber end-face and figure 3.6.b belongs to the same fiber after laser radiation was applied. The images were taken in the differential interference contrast (DIC) mode. The cracks and scratches cause light scattering from the tip, and thanks to the laser polishing, all cracks were eliminated and the scattering disapeared due to laser polished smooth surface.

3.3 Radial Fiber Optical Probe

The direction of the laser beam can be controlled by forming the fiber tip with appropriate geometry. Conical tip fiber emits the light radially. The deflection of laser beam is 360° with homogeneous ring shape around the fiber tip. Radial (360°) emission is useful for many minimal invasive medical operations inside the tubular organs. The shape of output beam strongly depends on the tip angle. Cone tip angle should be determined according to the characteristics of both the fiber and the laser. The cone tip angle must provide that the laser power coupled into the fiber exits with minimum loss and that all the power should be localized into the ring shape emission, not the same direction along the fiber. The homogeneous ring shape laser emission provides homogeneous photothermal destruction inside the tubular organs, therefore, only the desired tissues are eliminated by laser ablation [51].

Cone tip fiber is encapsulated in a glass capillary to avoid tissue pieces and other materials from damaging the tip shape which causes a change in laser deflection. It is also important to protect the body from any damage which can originate from any possible fiber tip breaks [52]. In this section, the aim is to examine the cone shape optical fiber tip in terms of ray tracing and modelling in order to decide the appropriate cone angle for fibers having core/cladding/coating diameter 600/630/1040 μm fibers [53]. The ray tracing theory is combined with experimental results to fabricate the perfect radial fiber. It is also an important challenge to fabricate radial fibers with a fine end-face surface. The surface roughness for each lapping film are represented and the light deflection calculations and measurements are explained. Mechanical polishing is a common fabrication procedure. However, as mentioned before, it is a time consuming and laborer dependent process. Although smooth surface roughness can be achieved by mechanical polishing technique, there is another way to polish cone tip, CO_2 laser polishing. Laser polishing process takes less time and it is completely independent from laborer. However, the tip shape cannot be completely formed by $continuouswave(cw) - CO_2$ laser. The solution is to combine these two polishing techniques to reduce the spent time on lapping films and eliminate the laborer dependence. The shape of the cone tip was formed first by mechanical rough-polishing and the laser radiation was, then, exposed to the tip to make it smoother. Light deflection measurements, SEM and AFM analysis were performed to show the changes in the radial tip fiber before and after the laser irradiation.

In this study, the main application of the modelled, fabricated and tested cone-shaped fiber optical probes is the treatment of venous reflux, which is a very common disease. Approximately 55% of women and 45% of men suffer from symptoms such as fatigue, pain and swelling of lower limbs [51]. Hormonal changes, standing or sitting for a long time might lead to this disease. The venous reflux is completely treated by laser ablation method using radial fiber probes. Laser system for this application was built by our research group and E-A Teknoloji Biyomedikal Cihazlar Dijital ve Optik Sistemler Nanoteknoloji Ar-Ge İth. İhr. Taah. San. ve Tic. Ltd. Şti. and the tests of the laser device is represented in $Chapter-4$.

3.3.1 Ray Tracing

Ray tracing can be divided into 3 possible geometries. These geometries were explained by using total internal reflection, partial reflection and refraction and the ray deflection from conical tip was formulized [54]. In order to simplify the ray tracing system, rays are traced parallel to the tip. The side-firing deflection is represented in figure 3.7.a. Incoming ray is reflected (according to TIR) from first side of the fiber tip, and refracted from second side of the tip. In figure 3.7.b, incoming ray is reflected from both sides of the fiber tip and totally back reflected. In this case, ray cannot be deflected from fiber tip. In figure 3.7.c, ray refracted from first side of fiber tip without reflecting.

Relation for these cases can be written as equations below:

Relation for 3.7.a:

$$\psi < \pi - 2\theta_{critical} \tag{3.1}$$

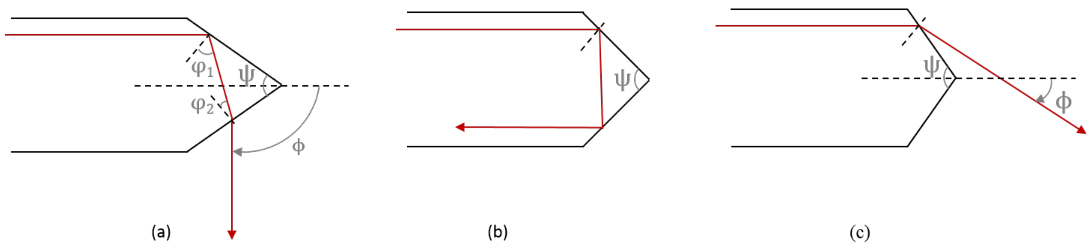

Figure 3.7: Ray tracing analysis for conical tip fiber.

Relation for 3.7.b:

$$\pi - 2\theta_{critical} > \psi > \frac{\pi + \theta_{critical}}{3} \tag{3.2}$$

Relation for 3.7.c:

$$\psi > \pi - 2\theta_{critical} \tag{3.3}$$

$\theta_{critical}$ for $n_{core} - n_{air}$ boundary can be calculated as 43.6° by using equation 2.2. Deflection angle versus tip angle relation for case (a) can be calculated as:

$$\phi = \frac{\pi - \psi}{2} + \arcsin(\frac{n_{core}}{n_{air}} \sin\varphi_2) \tag{3.4}$$

Deflection angle versus tip angle relation for case (c) can be calculated as:

$$\phi = \arcsin(\frac{n_{core}}{n_{air}} \sin\varphi_1) - \varphi_1 \tag{3.5}$$

Deflection angle versus tip angle relation cannot be calculated since arcsin does not have values for case (b).

3.3.2 Zemax Modelling

Ray tracing analysis was studied by Zemax in non-sequential mode for radial fiber. Fiber geometry was constructed so that the core/cladding diameter of the fiber was 600/300 micrometer, the NA of the fiber was 0.39, the NA of the light source was 0.22 and the wavelength of incoming rays was 635 nm. 100000 rays were analyzed and 100 rays are shown in figure 3.8.a and in figure 3.8b., radial diffusion is shown when hemi-spherical dedector is put inside the fiber tip. The tip angle was formed at 60° to observe the light deflection from the tip.

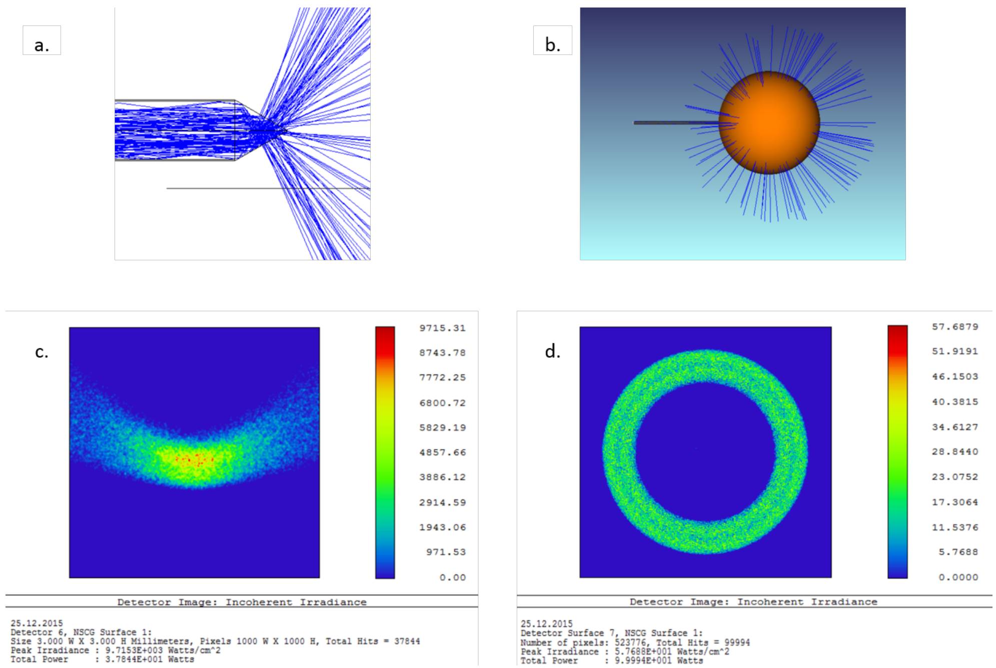

Figure 3.8: Zemax ray tracing simulation for radial fiber.

In figure 3.8.c, rectangular dedector image, which shows the spatial beam profile of the radial fiber tip, is represented. In figure 3.8.d, the ring-shaped beam profile is shown in hemi-spherical detector surface and the perfect ring shape can be obtained when the tip angle is chosen as 60°.

3.3.3 Fabrication and Light Deflection Measurements

In order to obtain circular beam, the fiber tip was formed with cone-shaped geometry. Cone-shaped fiber tips were fabricated by polishing on aluminum oxide particle coated lapping films. Mechanical and CO_2 laser polishing were both applied in this study.

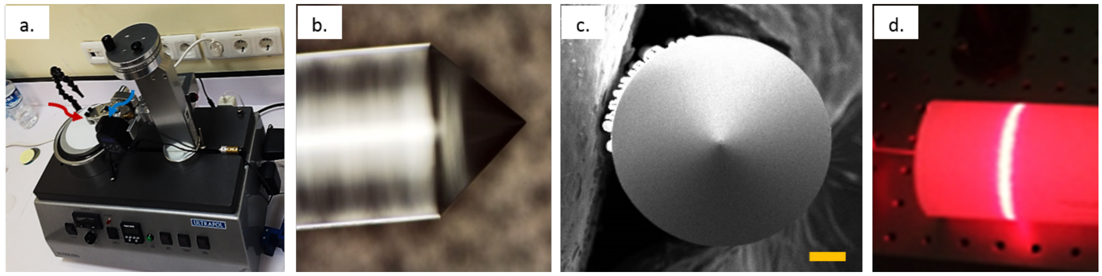

Figure 3.9: Fabrication procedure of the side-firing fiber probe. (a) Polishing procedure, (b) optical microscope image, (c) SEM image (scale bar: $100\mu m$), (d) spatial distribution of radial probe.

The polishing machine (Ultrapol, USA) represented in 3.9.a was used for mechanical polishing process. The red arrow indicates the turning table which has a lapping film on the top side and the blue arrow indicates the fiber holder. The tip angle can vary by changing the slope of the fiber holder and the detector displays the exact angle. Side-firing and radial fiber probe tips can be fabricated by this polishing machine since both the lapping film and the fiber holder are allowed to rotate. Also, the rotation speed can be altered. Optical microscope image and SEM image of the radial fiber tip are represented in figure 3.9.b and 3.9.c, respectively. In figure 3.9.d, circular beam distribution of radial fiber tip is demonstrated. The fabrication process will be explained in the next section in detail.

3.3.3.1 Mechanical Polishing

Fibers used in this process had $600/630/1040\mu m$ core/cladding/coating diameter. The cleaved, flat-ended fiber was inserted inside the fiber holder as shown in figure 3.9.a and the angle was set to 60°. Rough-lapping film ($30\mu m$) was sticked on the turning table, and started to rotate around its axis. The fiber tip approached to the rotating lapping film gently. The lapping film cause an abrasion on the end-face of the fiber tip, then the forming of the tip shape began. After the tip is formed by the rough film, the fine polishing step is started with the lapping films having lower surface roughness with $9\mu m, 3\mu m\ and\ 0.3\mu m$. SEM images of fibers polished with films having roughness (a) $30\mu m$, (b) $9\mu m$, (c) $3\mu m$ and (d)

$0.3\mu m$ in figure 3.10 respectively.

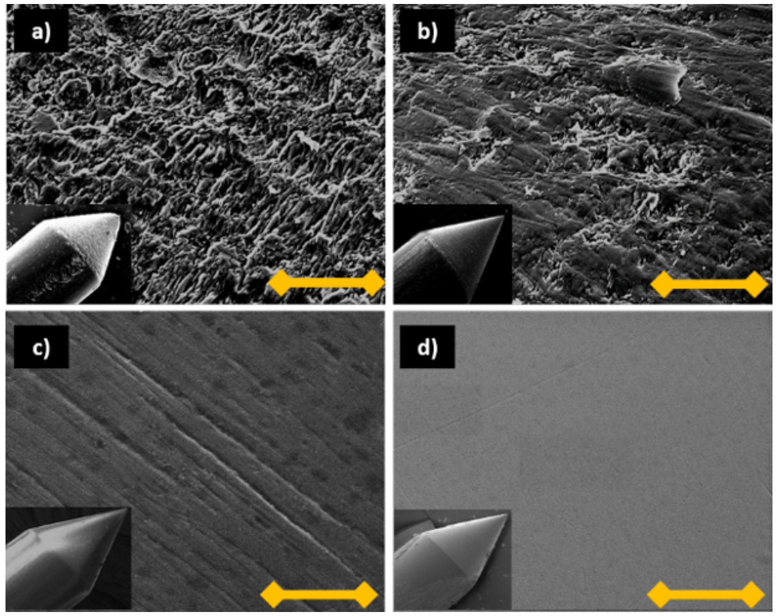

Figure 3.10: SEM images of optical fiber surfaces after polished at (a) $30\mu m$, (b) $9\mu m$, (c) $3\mu m$, (d) $0.3\mu m$ films. (Scale bar: $5\mu m$)

Rough lapping film ($30\mu m$) provides forming the fiber tip shape. However, its surface was not enough to be used in an operation (EVLA) and it was aimed to make it smoother in the subsequent steps. As shown in the figures 3.10, the surface roughness was gradually reduced with the applied lapping film roughness and, finally, smooth surface was achieved.

In order to emphasize the effect of the fiber tip surface roughness on the light deflection, an in-house built set up was used to measure the light deflection. In figure 3.11.a, the schematic representation of the setup is shown. The fiber tip is positioned in the center of the detector's circular path. The detector was allowed to rotate in the range between $-90° \; and + 90°$. The detector rotates around the fiber tip while recording the power value. The resolution was 1° meaning that the power value was recorded at each degree. In figure 3.11.b, the deflection angle versus tip angle graph is shown. In the ray tracing part, the deflection from the tip characteristics due to tip angle was examined and the deflection angle was determined for each possibilities. The relation between the tip angle and the light deflection angle is indicated in this figure. There were three functions to

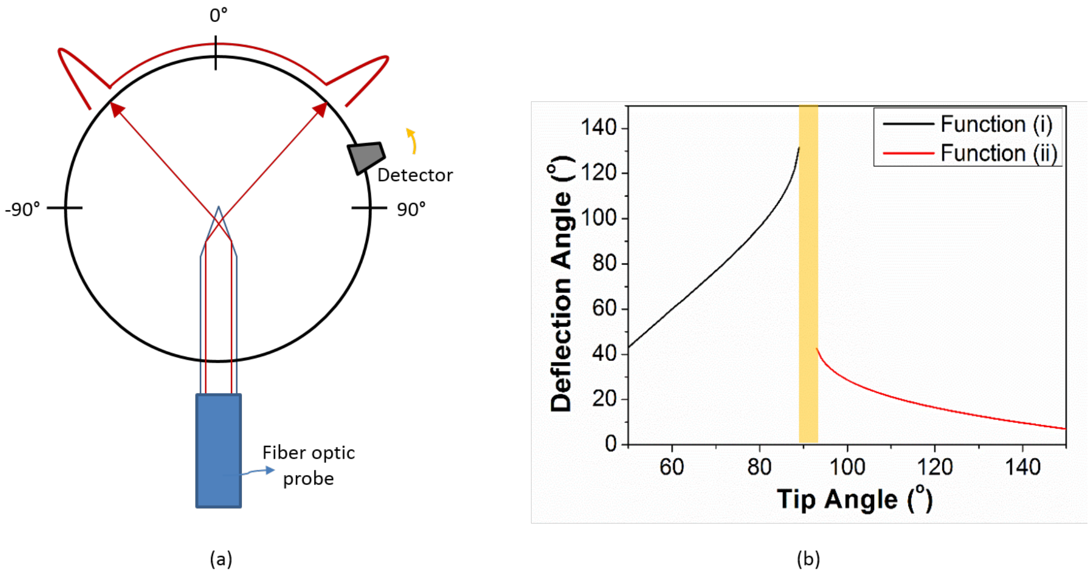

Figure 3.11: (a) Scheme of light deflection measurement setup for conical fiber. (b) Graph of deflection angle versus tip angle.

explain the light behavior: function (i) refers to equation 3.4, the function (ii) refers to 3.5 and the yellow discontinuity region refers to relation 3.2 . This graph was plotted according to these equations while n_{core} was 1.4501 and $n_{cladding}$ was 1.3923.

The light deflection differs due to roughness of the fiber surface. The rougher the fiber surface, the more the light diffuses. The cone-tips having smooth surface roughness are inserted into a glass capillary by fusing with gas-oxygen torch as shown in figure 3.12.a. The beam profiler image is shown in figure 3.12.b. In figure 3.12.c, the graphs are plotted for fiber tips polished at (i) $30\mu m$, (ii) $9\mu m$, (iii) $3\mu m$ and (iv) $0.3\mu m$ lapping films. The tip angle of the fabricated fiber was $60°$ and its deflection should be at $60°$. The peak power increases due to reduced surface of fiber tip. The the smaller beam width obtained when the roughness was diseapeared due to fine polishing. Also, deflected laser beam was located at $60°$ as calculated when $n_{core} = 1.45$, $n_{core} = 1$ and tip angle $\psi = 60°$ using equation 3.4. The final product of radial fiber probes were developed by our group and company. This product is succesfully applied in an EVLA operation and now commercially available.

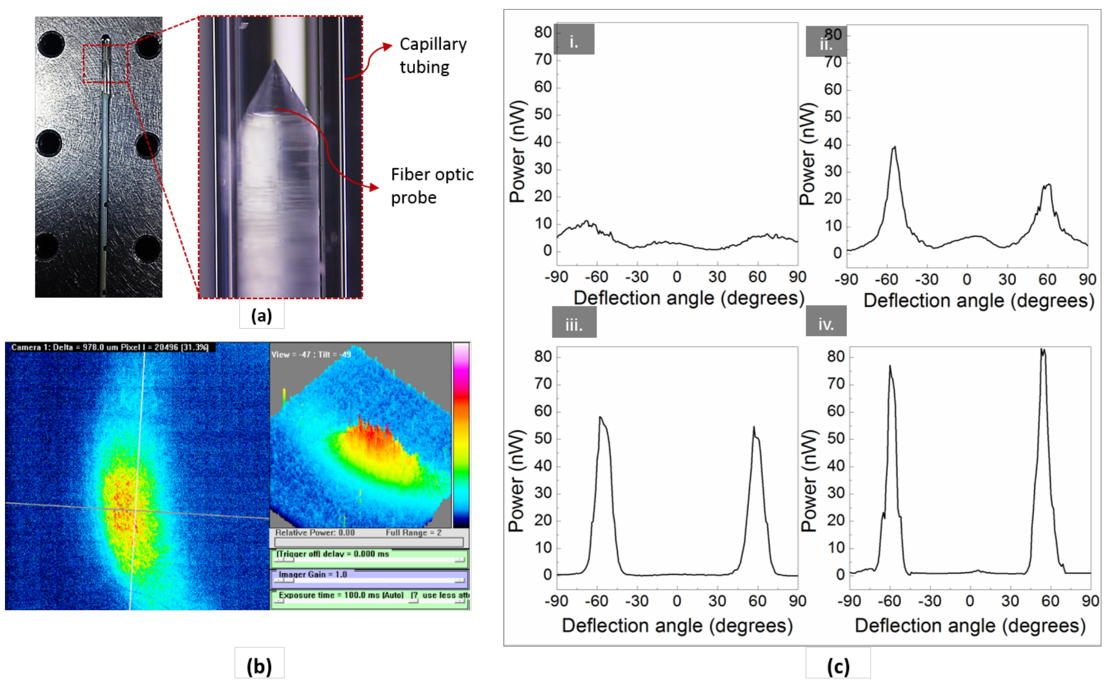

Figure 3.12: (a) The final form of the tip of the radial fiber probe, (b) beam profile of radial optical probe. SEM images of optical fiber surfaces after polished at (i) $30\mu m$, (ii) $9\mu m$, (iii) $3\mu m$, (iv) $0.3\mu m$ films.

3.3.3.2 Laser Polishing

The conical fiber tips were exposed to CO_2 laser radiation after the tip shapes were formed by mechanical polishing. The LZM100(AFL) was used as mentioned before. The laser power was modulated by using shutter (shown in figure 3.5) as a chopper. The function which modulated the laser beam was written into the device. It was composed of 8 pulses of laser energy with $1s$ duration and 1s interval. Laser power density was $9.15x10^3 \frac{W}{cm^2}$. These parameters were optimized due to laser polishing of the flat-ended fiber tip. The SEM images of laser polishing of radial fibers polished at $30\mu m$ and $9\mu m$ films and then processed with CO_2 (a) and (b) are shown in the figure 3.13. In figure 3.14, surface roughness images taken by AFM are represented. In figure 3.14, (a) fine mechanical polished fiber surface is shown with $1.17nm$, CO_2 treated fiber tips after polished with (b) $9\mu m$ film with $3.38nm$, (c) $30\mu m$ film with $7.87nm$ average roughness. In the literature, Udrea *et al.* obtained $100nm$ average surface roughness of fiber end-face surface after polishing with cw-CO_2 [48].

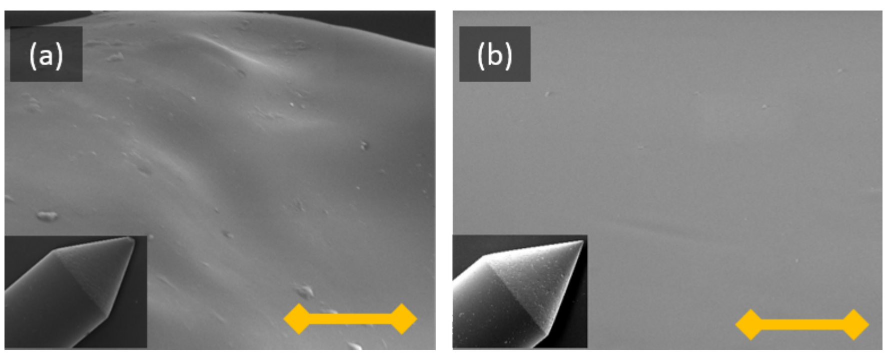

Figure 3.13: SEM images of CO_2 laser treated fiber tips after polished at: (a) $30\mu m$, (b) $9\mu m$ films. (a) $30\mu m$, (b) $9\mu m$ films. (Scale bar: $5\mu m$)

Also, in order to clarify the effect of the roughness to the intensity, the measurements were performed for both steps. Light deflection graphs for the fiber tips, which were laser processed after polishing on $30\mu m$ and $9\mu m$ films, are shown in figures 3.15.a and 3.15.b, respectively. The light deflection measurements for each case have less power intensity after mechanical polishing was applied. For

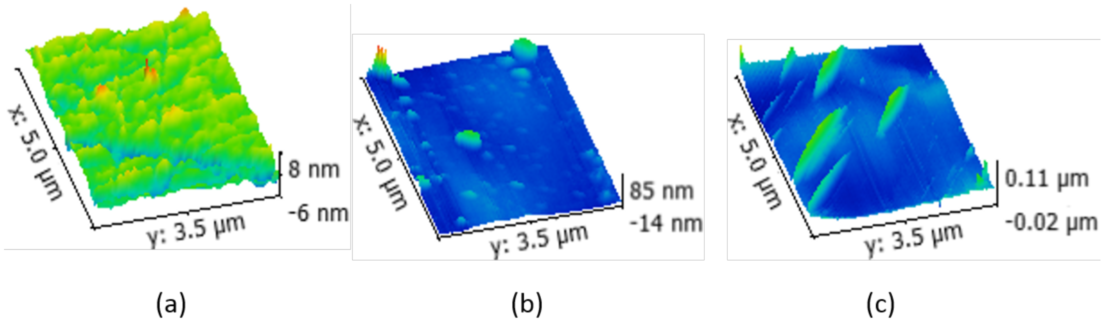

Figure 3.14: AFM images of (a) fine mechanical polished, CO_2 laser treated fiber tips after polished at: (b) $9\mu m$, (c) $30\mu m$ films.

each case, the power increases after laser polishing was applied. Thus, the laborer dependent and time-consuming steps were skipped thanks to the CO_2 laser polishing.

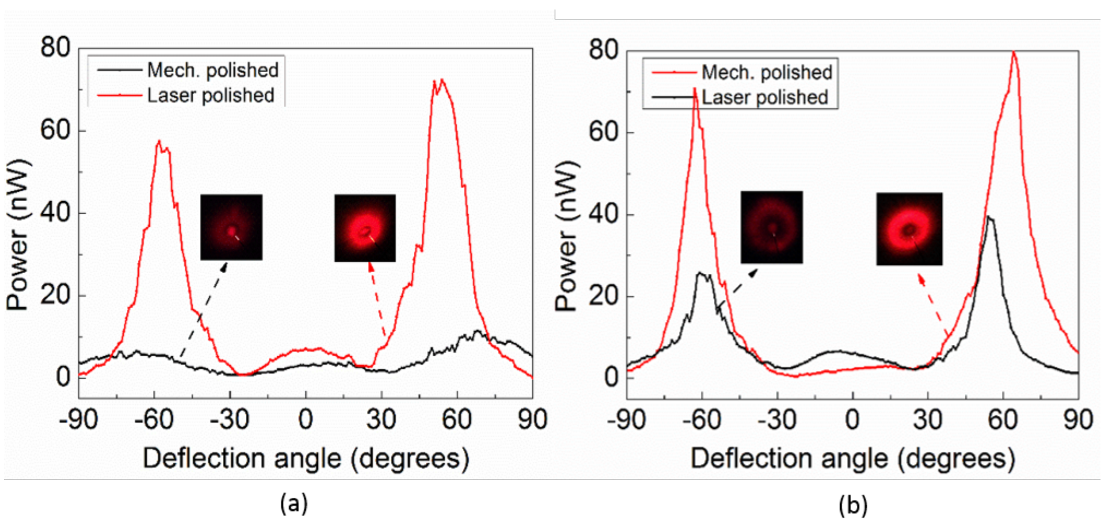

Figure 3.15: Deflection measurements CO_2 laser treated fiber tips after polished at: (a) $30\mu m$, (b) $9\mu m$ films.

3.4 Double-Ring Radial Fiber Optical Probe

Double ring fiber optic probe has a modified cone-shaped tip geometry. It splits the laser power into two rings. Double ring light deflection is very effective for endovenous laser ablation (EVLA) operation. The burning effect is reduced due to less energy density of each ring. Also, the first ring playing as a pre-heater role which allows to pre-shrink the vein and ablation process becomes more effective. A patented commercial product is available in the Biolitec (Germany). The geometry of the tip is composed of two cones with different cone angles. First cone is polished from the tip through the middle of the cone and its shape becomes flat-ended equilateral parallelogram. The second tip is spliced to flat side of the end of the first tip [55]. The process includes polishing, splicing, and cleaving which are not easy steps. In our group, we produced, modelled, and measured home-made double ring fiber probe which was fabricated by another technique. It is an ongoing project to commercialize this product by getting its patent. Therefore, we are not able to show the tip geometry, but the Zemax modelling and light deflection measurements are represented in this study.

3.4.1 Zemax Modelling

Ray tracing analysis is studied by Zemax in non-sequential form for double-ring radial fiber. Fiber geometry was constructed so that the core/cladding diameter of the fiber was 600/630, the NA of the fiber was 0.39, NA of the light source was 0.22 and the wavelength of the incoming rays was 635nm. 100000 rays were analyzed, 100 rays are shown in figure 3.16.a and in figure 3.16.b, double-radial emitting tip is shown when hemi-spherical dedector is put outside of the fiber tip.

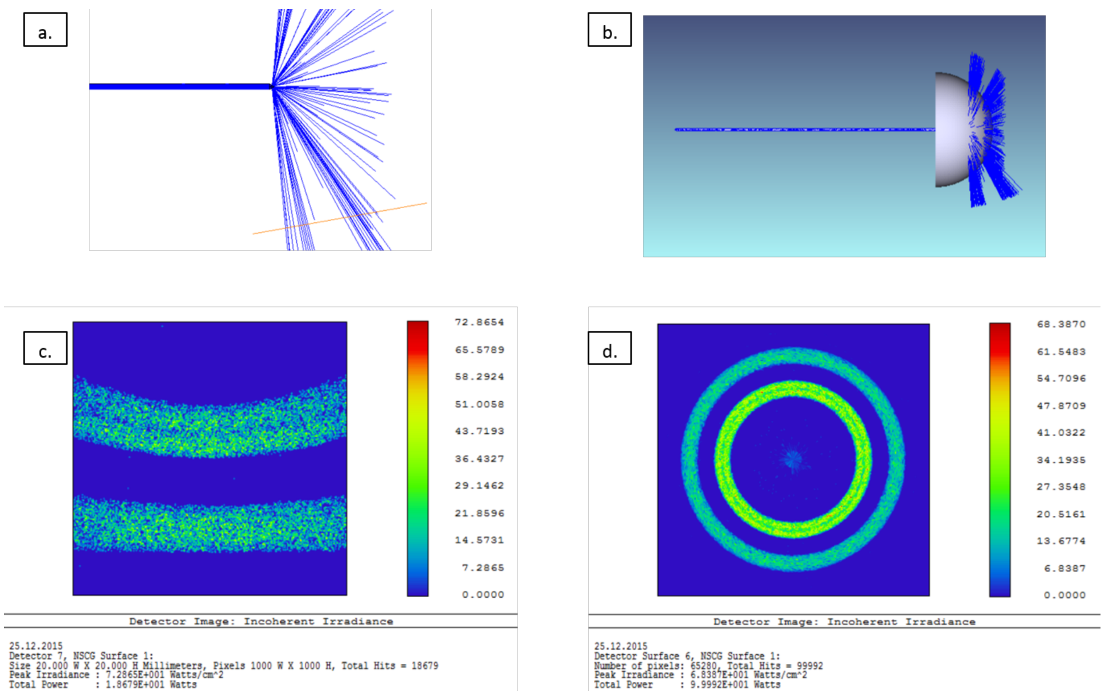

Figure 3.16: Zemax ray tracing simulation for double-ring radial fiber.

3.4.2 Light Deflection Measurements

Double-ring emitting fiber tip is formed by mechanical polishing. Light deflection measurements were taken in the setup shown in figure 3.11.a. The laser beam coming inside the optical fiber, splits into two beams when exits from the modified fiber tip. In figure 3.17.a, demonstration of double ring emitting fiber is represented. Two beams can easily be seen image taken by beam profiler in 3.17.b. In graph 3.17.c, double-ring pattern is shown. We also proposed that the power distribution can be altered due to geometry of the fiber tip.

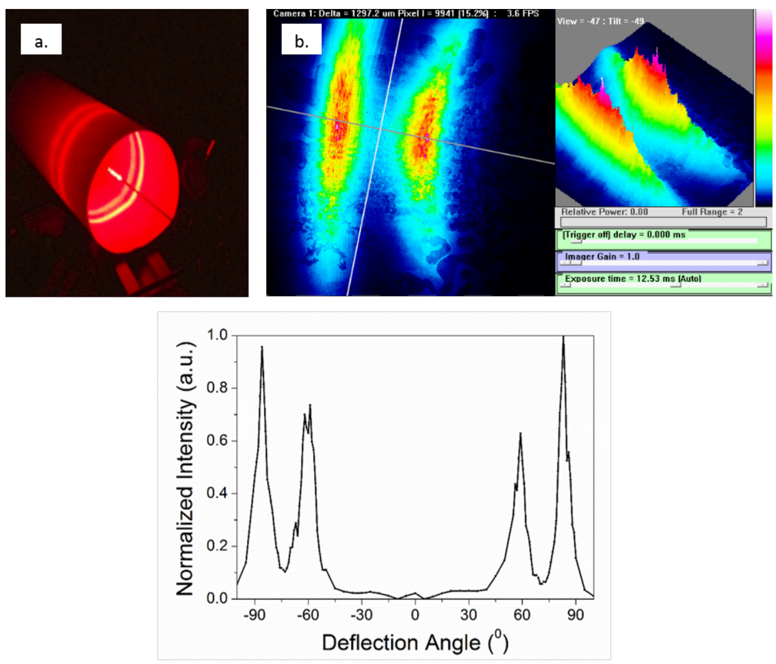

(c)

Figure 3.17: Light deflection measurements. (a) Spatial distribution, (b) beam profiler, (c) light deflection measurements of double ring radial fiber-optic prob.

3.5 Side-Firing Fiber Optic Probe

Side-firing fiber optical probes are important tools in laser medicine. In the case of flat-ended fiber probes, light is transmitted as coupled out in the direction of the fiber. The deflected light direction can be controlled by changing the fiber end-surface shape. Laser beam can be emitted almost perpendicular to the fiber axis thanks to the side-firing fiber probes. The main idea is that the laser beam can be localized onto the area that is desired to be ablated. It is very important to transmit almost full power of the laser perpendically, however, the light is coupled out from the fiber tip in three ways: leakage, deflection with leakage and perpendicularly deflection from the fiber tip [56]. In order to reduce the leakage from the tip, the tip angle should be chosen specifically (this concept is explained in the ray tracing part). It is desirable to fabricate a side-firing probe without any leakage. This is important for the medical applications since the laser beam leakage could damage healthy part of the tissue. The side-firing probes are used in the medical applications. They are suitable for the removal of tissue in hollow organs. These probes are desired for urology applications. Prostate tumors can be ablated thanks to side-firing probes [34]. There are studies suggesting that small breast cancer tumors can also be eliminated using these probes [33].

3.5.1 Ray Tracing

A slanted end-face geometry of fiber provides a light beam which is directed through side of fiber tip. The tip angle is crucial to deflect maximum power without loss. Thus, Brewster angle at the air-fiber boundary should be calculated as shown in equation 3.6, when n_2 stands for air and n_1 is considered as refractive index value of the fiber core:

$$\arctan \frac{n_2}{n_1} = \arctan \frac{1}{1.45} = 34.21^\circ \tag{3.6}$$

The Brewster angle results in a total reflection from air-fiber boundary. Thus, the tip angle should be 34.21° to obtain total internal reflection without any loss and all the laser beam is emitted through the side of the fiber theoretically. In a study conducted by Falk and Pashaie (2013), the tip angle for side-firing probe was calculated that the angle should be smaller than 38° for fiber having NA 0.22 using these calculations.

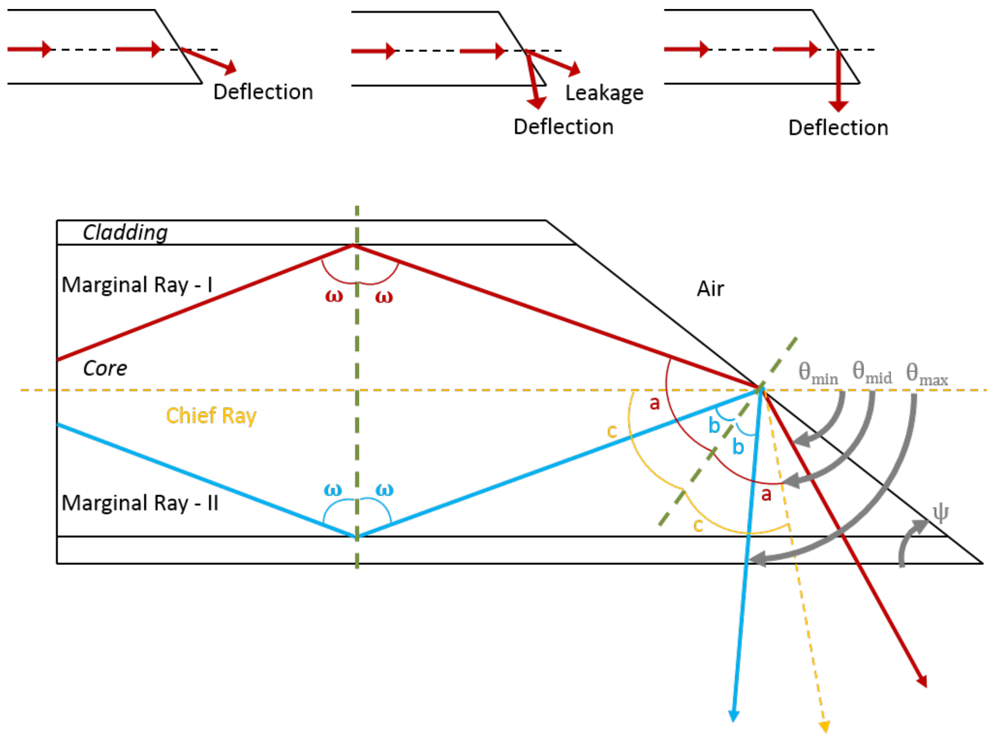

Figure 3.18: Ray tracing analysis for side-firing fiber tip.

In figure 3.18, ray tracing analysis is illustrated. The deflection angle depends on tip angle of the fiber [56]. Deflection angle and tip angle relation can be extracted by ray tracing analysis and from fiber tip geometrical relations. For marginal ray - I, θ_{max} can be calculated by using equation 2.1 and 2.2:

$$\psi = \omega - b \tag{3.7}$$

$$\theta = 2\psi + (90 - \omega) \tag{3.8}$$

$$\theta_{max} = 2\psi + (90 - \omega'_{critical}) \quad (3.9)$$

The marginal ray - II can also be calculated as:

$$\psi = 180 - (\omega + b) \quad (3.10)$$

$$\theta = 2\psi - (90 - \omega) \quad (3.11)$$

$$\theta_{min} = 2\psi - (90 - \omega'_{critical}) \quad (3.12)$$

The angle between n_{core} and $n_{cladding}$, ω should be larger than critical angle which is calculated by the equation 3.14, and ω should satisfy $\omega'_{critical} < \omega < 90°$. From the tip angle calculation, we found that tip angle should be $\sim 34°$ in equation 3.6. The divergence lobe ($\triangle\theta$) can be found as:

$$\triangle\theta = \theta_{max} - \theta_{min} = 180 - \omega'_{critical} \quad (3.13)$$

3.5.2 Zemax Modelling

Ray tracing analysis was carried out by Zemax in non-sequential form for side-firing fiber. Fiber geometry was constructed so that the core/cladding diameter of the fiber was 600/630 micrometer, the NA of the fiber was 0.39, the NA of the light source was 0.22 and the wavelength of incoming rays was 635nm. 100000 rays were analyzed and 100 rays are shown in figures 3.19.a and b. The tip angle was set at $\sim 34°$ to observe the light deflection from the calculated fiber tip.

In figure 3.19.c, rectangular dedector image, which shows the spatial beam profile of the side-firing fiber tip, is represented. 80% of the incoming rays are

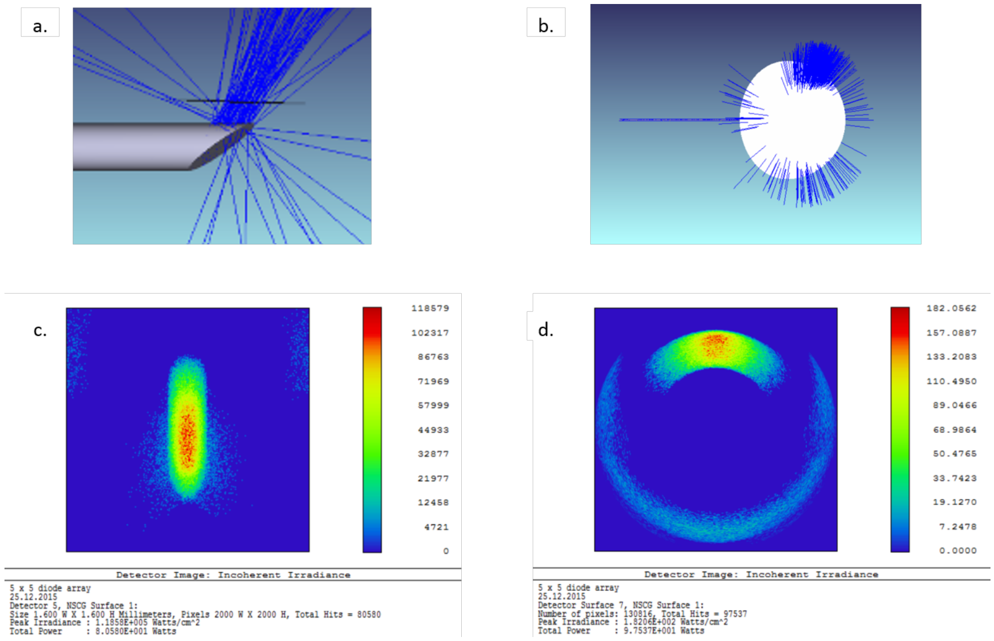

Figure 3.19: Zemax ray tracing simulation for side-firing fiber.

deflected and located onto the an area. 80% can be achieved but 100% cannot be possible since we have a multi-mode fiber. In figure 3.19.d, the localized beam profile is shown in hemi-spherical detector surface.

3.5.3 Fabrication

KrellTech polishing machine was used for this process. The procedure was almost the same as the one applied to the radial fiber tips in the section 3.3.3.1. The only difference was that the fiber did not rotate around its center in order to form side-firing probe shape. The optical fiber (diameter of core/clad is 600/630 μm) was inserted inside KrellTech fiber holder. In figure 3.20.a, KrellTech polishing machine and the fabrication procedure is shown. The blue arrow indicates the rotational stage, the angle of which can be set by turning it, and it is fixed to 56° to form a side-firing probe having tip angle 34°. The red arrow shows the fiber holder. The rotational speed was also adjustable for this polishing machine. In figure 3.20.b, the camera display is shown for the positioned fiber tip before the polishing. The polished side-firing tip is represented in figure 3.20.c. The light deflection measurement is demonstrated in the figure 3.20.d.

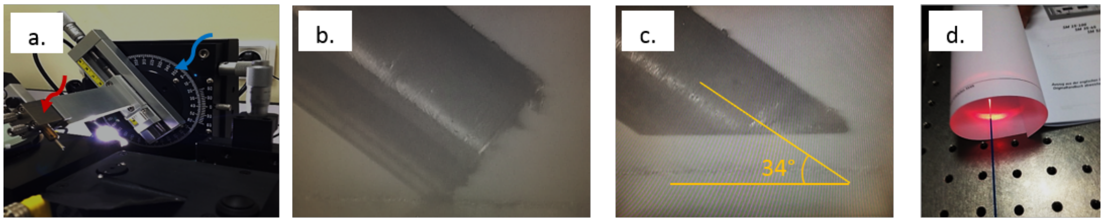

Figure 3.20: Fabrication procedure of the side-firing fiber prob. (a) Polishing procedure, (b) before polishing, (c) after polishing, (d) spatial distribution of side-firing probe.

3.5.4 Light Deflection Measurements

The light deflection measurement setup is represented in figure 3.21.a. The data recording process was almost same as the process of radial fiber light deflection. Only difference was that the light deflection of the side-firing fiber was located onto one spot. In figure 3.21.b, the relation between deflection angle versus tip angle is plotted by using the ray tracing calculations and equation 3.13.

In figure 3.22.a, beam profiler image of laser beam is represented. Light deflection measurements were taken in the setup shown in figure 3.21.a. In figure 3.22.b, the light deflection of the side-firing fiber was plotted when tip angle is 34°. As seen from the figure 3.22.b, the spatial distribution of laser deflected from the fiber is located approximately at 55°. The graph in figure 3.21.b confirms the light deflection angle due to tip angle with a few degrees error.

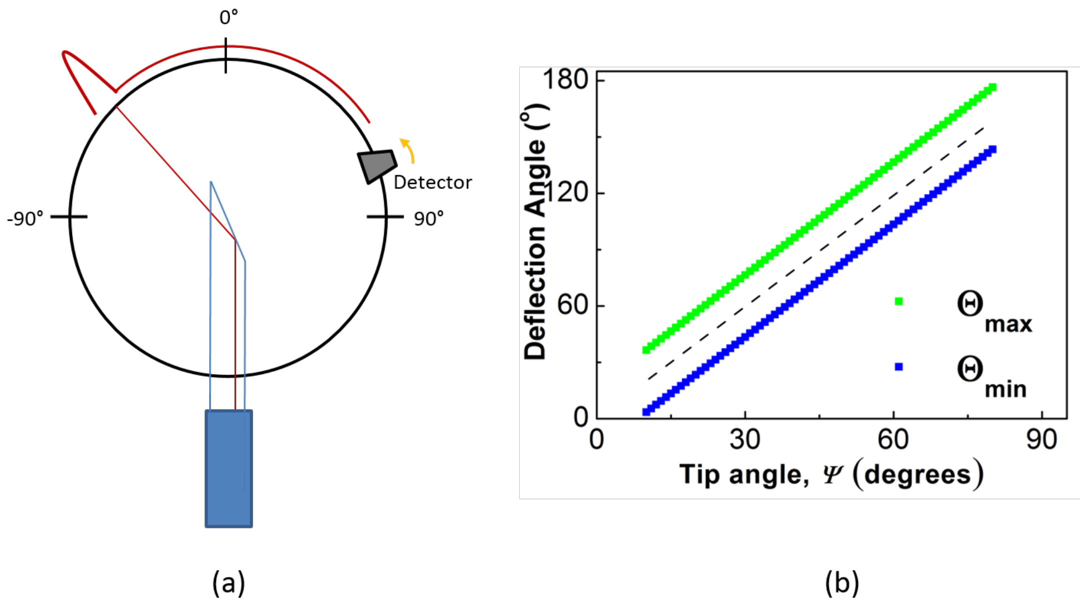

Figure 3.21: (a) Scheme of light deflection measurement setup for side-firing fiber. (b) Graph of deflection angle versus tip angle.

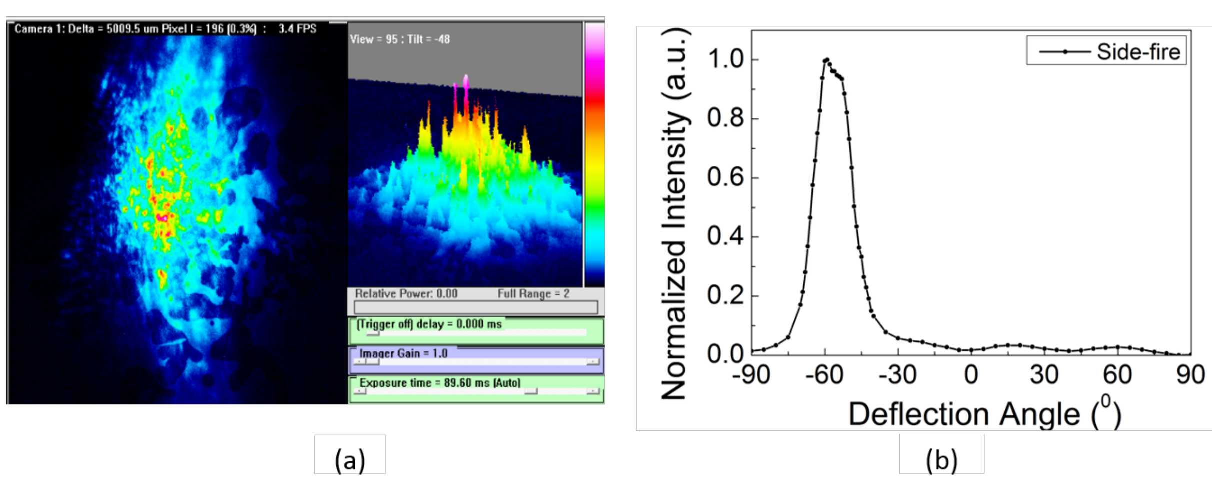

Figure 3.22: Measurements for side-firing fiber probe: (a) beam profiler image, (b) light deflection distribution of side-firing probe.

3.6 Flat-ended Fiber Optic Probe

Flat-ended fiber optic probes have a basic geometry and used in a number of fields. Fiber laser systems, medical applications, imaging optics and fiber optic telecommunication are some of the fields that flat-ended fiber optic probes are used. They are also used in photodynamic theraphy which is a gentle form of tumor treatment. In this study, the flat-ended fiber probe was examined in terms of ray tracing, Zemax modelling and light deflection. The probe was fabricated by mechanical polishing process.

3.6.1 Ray Tracing

Ray tracing analysis for flat-ended fiber was studied according to critical angle, total internal reflection (TIR), numerical aperture (NA) and acceptance angle as shown in figure 3.23. Critical angle between core and cladding can be found by equation 2.3, thus the angle ω is larger than 73.45° :

$$\theta_c = \arcsin(\frac{1.39}{1.45}) = 73.45° \tag{3.14}$$

Rays exit the fiber due to fiber characteristics. In our analysis, fiber having core/clad diameter 600/630 μm , NA 0.39 was used. Rays exit the fiber in the same direction with the fiber due to flat end-face geometry. The cone-angle becomes 22.9° using equation 2.6:

$$\theta = \arcsin(\frac{0.39}{1}) = 22.9° \tag{3.15}$$

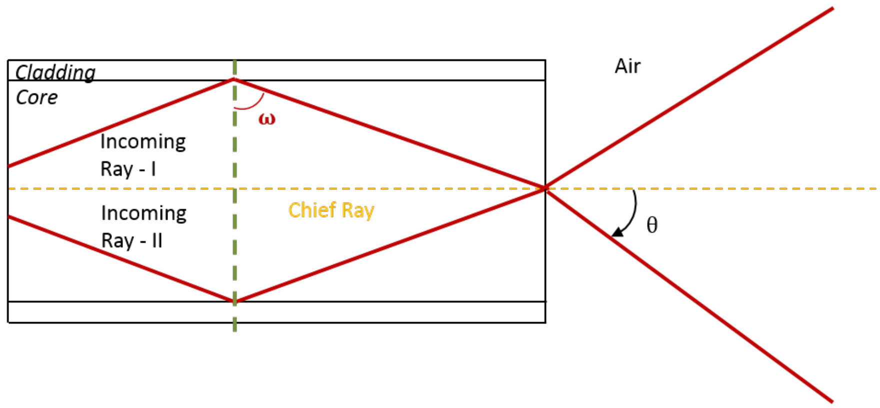

Figure 3.23: Ray tracing for flat-ended fiber.

3.6.2 Zemax Modelling

Ray tracing was modelled by Zemax in non-sequential mode for flat-ended fiber. Fiber geometry was constructed as 600/630μm core/cladding diameter, NA for fiber was 0.39, NA for light source was 0.22, wavelength of the incoming rays was 635nm. 100000 rays were analyzed, 100 rays are shown in figures 3.24.a and b. Spatial beam profile of the source is shown in figure 3.24.c, and fiber is shown in figure 3.24.d. They both have a circular shape, but the shape of the fiber output is larger due to dedector distance from the tip since rays diverge.

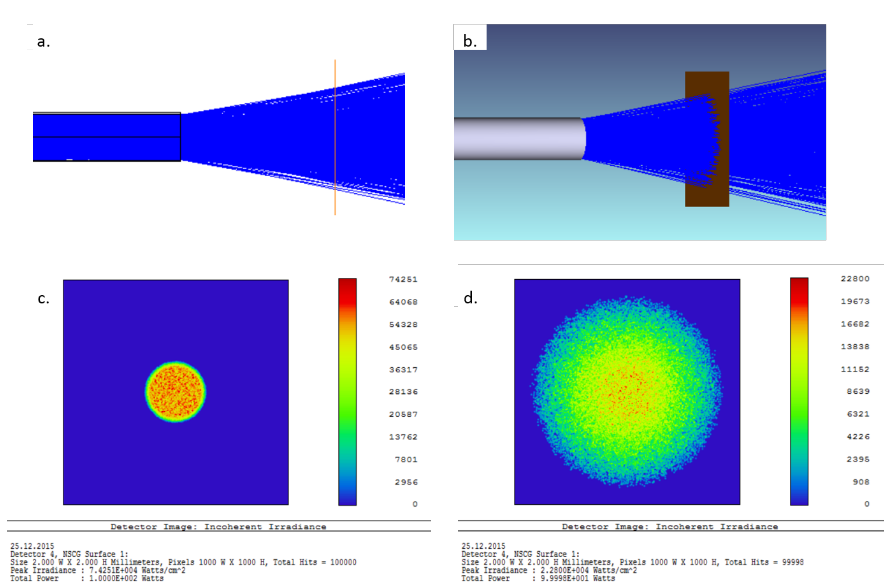

Figure 3.24: Zemax ray tracing simulation for flat-ended fiber.

3.6.3 Fabrication

The fiber end-face was formed by mechanical polishing technique as shown in figure 3.25.a. The fiber was positioned to the lapping film vertically in order to form flat-ended tip. In figure 3.25.b, side-camera image of the fiber is shown. The flat-ended tip structure was obtained after polishing process. Also, the surface roughness can be seen in bottom-camera image which is represented in figure 3.25.c. The light deflection of the flat-ended probe is in the same direction with the fiber. The laser beam is transmitted and deflected at the same direction. The demonstration of spatial beam profile of the fiber is shown in 3.25.d.

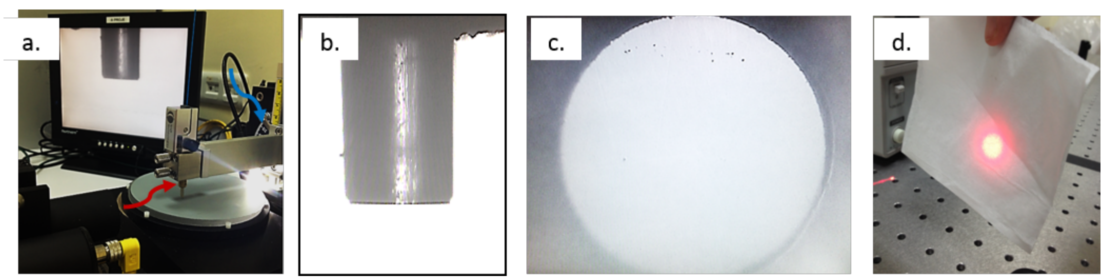

Figure 3.25: Fabrication procedure of the flat-ended fiber. (a) Polishing procedure, (b) fine polished and (d) spatial distribution of flat-ended prob.

3.6.4 Light Deflection Measurements

The light deflection measurements were taken in a home-made table-top setup, as shown in figure 3.26.a and b. These figures also belong to the schematic drawing of the measurement setups in figures 3.11.a and 3.21.a. The measurement setup was composed of a rotating stage, detector and fiber holder. Detector was fixed on the rotating stage. The rotating stage was fixed parallel onto the optical table. Optical fiber was put inside the fiber holder. The midpoint of the rotating stage and the tip of the optical fiber were placed as concentric. The detector revolved around the optical fiber tip while collecting the data. The light source is ThorLabs-S1FC635, 635nm. Distance between the tip and the detector was 46mm. The beam profile of the flat-ended fiber tip is shown in figure 3.26.c. The profile was observed as multi-mode. The fiber used in this measurement had core/clad diameter as 600/630 μm. In figure 3.26.d, deflection graph of the flat-ended fiber is shown. NA of the fiber was 0.39, and the acceptance half-cone angle is 20°. The intensity of illumination was determined as Gaussian and the half-cone angle was measured as approximately 20° experimentally.

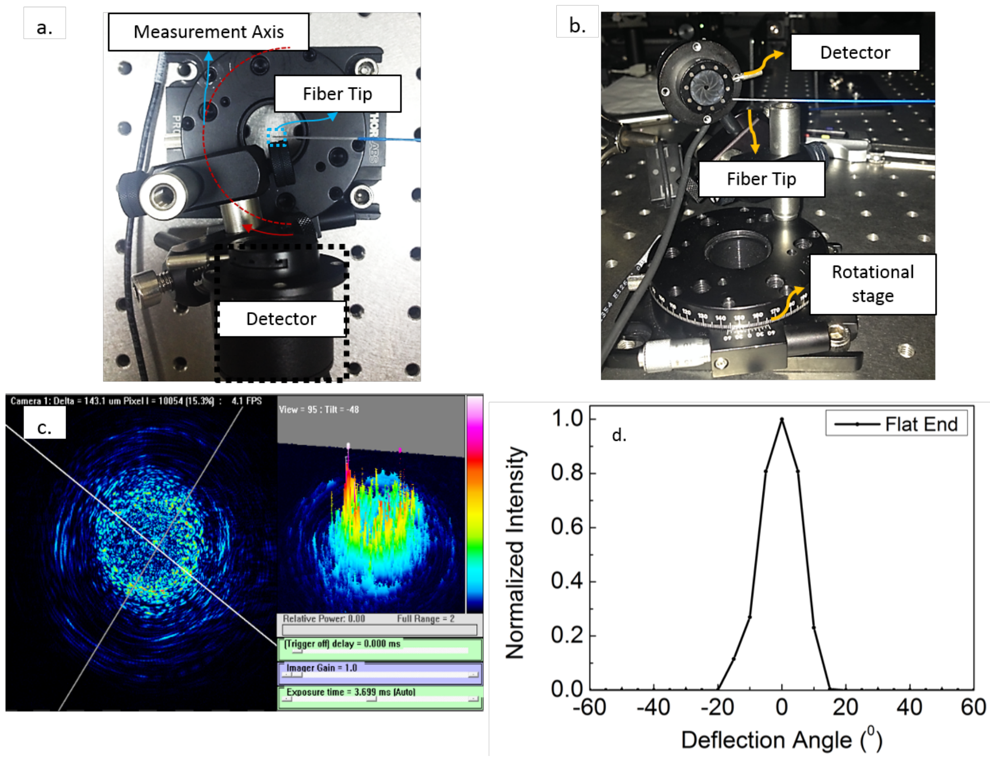

Figure 3.26: Light deflection measurement setup (a) top-image and (b) side-image. Measurments: (c) beam profiler image, (d) deflection graph of flat-ended probe.

3.7 Fabrication of Fiber Optic Connector

Fibers are ended up with connectors. Connectors are pieces which are fixed with epoxy onto the fibers to provide them rapid coupling of laser and fiber optical probe. These devices must be fabricated with a precision in order to plug in and out the fiber to the laser without disturbing the alignment of the optical system [57]. Also, connectors can provide coupling between two connectors. Hand polishing is used for fining the end-face of the fiber optic connector. In the

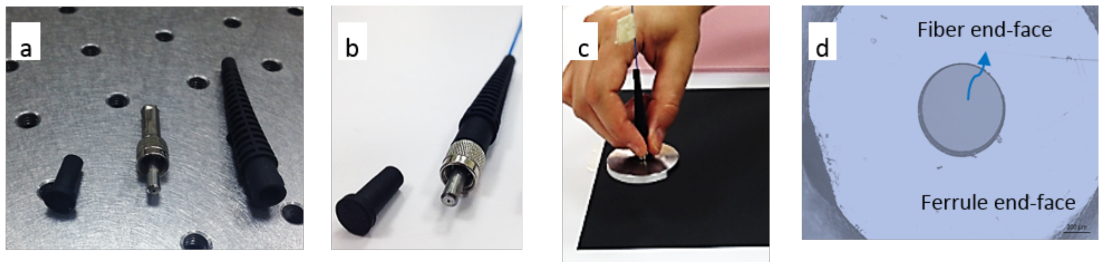

Figure 3.27: Optical fiber connector preparing procedure. (a) Connector components. ϕ $641\mu m$ bore (Steinless Steel ferrule), (b) after all components were epoxied, (c) hand-polishing of end-face of the ferrule, (d) optical microscope image of the connector end-face.

figure 3.27, fiber optical connector termination steps are briefly explained. In figure 3.27.a, $641\mu m$-bore diameter and steinless steel SMA connector parts are shown. In order to prepare fiber optical connector, first, approximately $2 - 3cm$ of the jacket was removed long by fiber stripping tool ($T28S31$) and clad/coating diameter was $630\mu m/780\mu m$. The bare fiber was cleaved with a ruby-tip fiber scribe. The cleaved bare fiber was inserted inside epoxy filled connector. Epoxy was the crucial material to fix fiber and connector together. The tip of the bare fiber was taken out approximately $0.5mm$ from the end-face of the connector. The aim of taking out some of the bare fiber from connector was to remove the epoxy residues from the end-face of the connector by polishing it. In figure 3.27.b, fiber was inserted into the connector and they are epoxied. After epoxy was dried, connector was ready for hand-polishing procedure. In figure 3.27.c, connectorized optical fiber is inserted inside SMA hand polishing disk ($Thorlabs - D50SMA$) in order to hold the fiber and ferrule end-face vertical to the polishing film. This procedure depends on the laborer. Fiber optical connector is polished on rough to fine lapping films. In figure 3.27.d, epoxied and hand-polished fiber optical connector end-face is shown. It is important to achieve both fiber and ferrule end-face smooth in the abrasion process.

3.8 Diffusing Fiber Optical Probe

Diffusing fiber probe provides homogeneous laser beam distribution around the tip and they are widely used in photodynamic theraphy. Microlens, baloon and cylindrical diffusers are commercially available products for photodynamic theraphy [58]. The fiber optical probes are used for activating the photo-sensitizer localized in the tumor tissue of the patient in order to initiate the phototoxic reaction. The tumor cells are destructed gently due to photodynamic theraphy [6]. In this study, diffuser probe fabrication process is represented. There is also one important application of diffusers for fiber laser systems. Diffusers can be used as a cladding light stripper (CLS) component in the fiber laser systems. They are used to extract cladding light from the fiber laser system by diffusing the cladding light out of the system. They improve the fiber laser system in terms of beam quality and robustness. CLS are also represented in this chapter.

3.8.1 Fabrication

Diffusing fiber probe emits the laser beam homogeneously along the bare fiber. In order to diffuse the laser beam, fiber surface is roughened with lateral mechanical polishing of the bare fiber side-surfaces. The rough poilshing crate abrasion on the glass surface and lead to random light scattering. This method is not easy to use since fiber becomes fragile when polishing. In figure 3.28.a, non-etched and etched fiber surfaces are represented. Etched fiber surface looks like frusty glass due to rough surface. In figure 3.28.b, light emitting from diffuser is illustrated. In figure 3.28.c, laser emission from diffusing fiber is demonstrated. A homogeneous laser distribution was obtained. In our study, roughened-fiber surface was used in fiber laser application since diffusers extract cladding light. Using this feature, diffusers can be used as cladding light strippers.

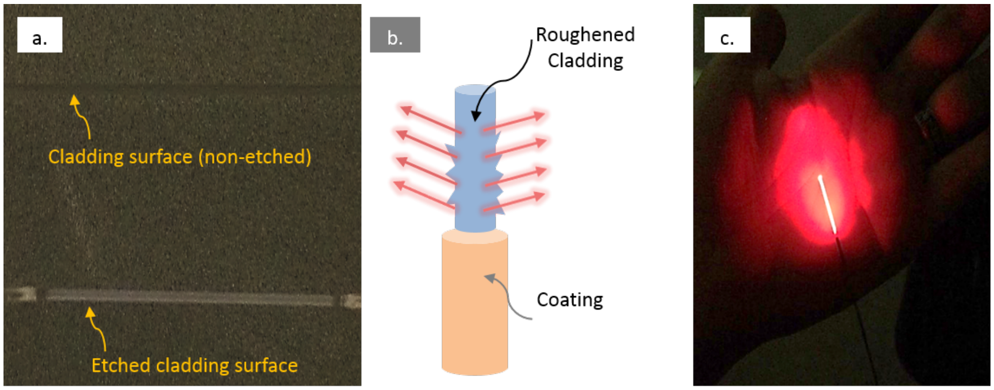

Figure 3.28: (a) Image of non-etched and etched cladding surface, (b) diffusion of light from etched fiber cladding, (c) demonstration of a diffuser fiber-optic prob.

3.8.2 High Power Laser Application: Cladding Light Strippers

Fiber lasers have attracted attention recently due to their high efficiency, low cost and working at high power regimes with high beam quality [59]. The important part of building fiber laser cavity is the integration such as splicing. The fiber optical parts must be spliced with a high quality. In order to prevent power loss and low signal beam quality, the cores and mode field diameter (MFD) must be matched during two fibers are spliced. Some of the signal light may leak into the cladding due to low-quality integration [60]. Also, some of the pump light could not be absorbed by active atoms inside the core. If the cladding light can not be removed from the system properly, several problems occur [61]. The cladding light can weaken the integration points and cause the cavity to get damaged. In fact, the cladding light can reach hunders of Watts. Also, the cladding light reduce the beam quality, M^2, which is an important parameter. In order to overcome these problems, the cladding light must be stripped without disturbing the system. There are several methods to strip cladding light such as high index polymer (HIP) coating and rough cladding surface [62], [63] . For the HIP-CLS case, total internal reflection from low index second cladding is violated since high index polymer is coated after stripping the low index polymer (second cladding). Therefore, cladding light is coupled into the HIP by the means of TIR without disturbing the core light. This type of CLS performance depends on the polymers' stability at high temperature. HIP coated CLS can handle 80-100W [64] . Another option to extract the cladding light is etching the first cladding in order to diffuse cladding light from the system. In this rough-CLS case, polymer is not used since it cannot handle high temperatures. However, optical fiber strength is reduced since roughing procedure weakens the fiber and there is no coating covering the cladding. In another CLS case, the cladding light is extracted from the system gradually to improve the thermal management occured in the polymer [65]. In our study, the rough CLS, rough and HIP coated CLS, HIP-CLS and cascaded CLS were examined. In figure 3.29, pump stripper

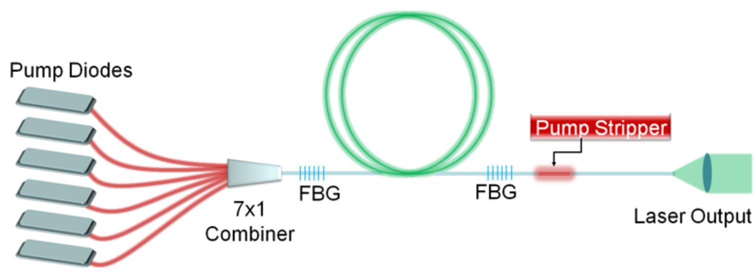

Figure 3.29: Fiber laser.

position is represented in fibe laser architecture and the red light indicates pump light and the green light indicates signal light. Pump diodes are inserted into the combiner. Active atoms inside the active fiber are excited by pump light and the laser signal is emitted. Active atoms could not absorb all of the pump light. Residual pump light is extracted from the fiber laser system without disturbing it thanks to cladding light stripper (or pump stripper).

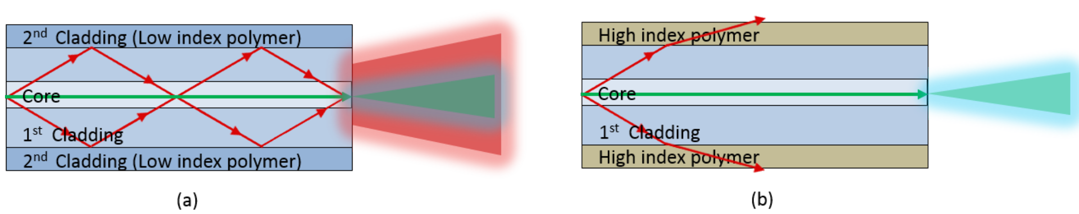

Figure 3.30: Double clad fiber laser output (a) without CLS, and (b) with CLS. (red light is pump and green light is signal light.)

Double cladding fiber structure and CLS applied to it are illustrated in figure 3.30. In figure 3.30.a, light guiding characteristics inside double clad is shown.

Pump light travels inside 1^{st} cladding while signal light is produced and travels inside the core. The output of the fiber contains both pump light and signal light. Pump light leads to a decrease in quality of the laser (M^2 value), as mentioned in section 3.8.2. In figure 3.30.b, CLS applied double clad fiber structure is represented. Cladding light is stripped by changing the fiber structure. Refractive index of the 2^{nd} cladding is less than refractive index of the 1^{st} cladding, thus, TIR is confirmed for structure shown in figure 3.30.a. High index polymer (HIP) is coated onto 1^{st} cladding instead of low-index coating. For HIP coated area, TIR is violated, and pump light starts to leak into the high-index polymer coating. Thus, pump light is extracted before reaching to output of the fiber laser and M^2 value is improved.

3.8.3 Fabrication and Characterization of Cladding Light Stripper

In our studies, four types of CLS were fabricated and characterized, namely rough, high index polymer coated rough, high index polymer coated and cascaded CLS. Rough CLS was fabricated by mechanical polishing after 2^{nd} cladding (low-index polymer) was removed. Other three types of CLSs were fabricated by high index polymer coating after 2^{nd} cladding is extracted from fiber surface. Refractive index of high index polymer was 1.539. HIP was a UV-curable material. Thus, it was UV-cured onto bare fiber surface after poured into molding. Experimental setup is represented in figure 3.31.a and the inset belongs to SolidWorks design of CLS-molding. In figure 3.31.b, schematic representation of the experimental setup is shown. Pump diode (Dilas, Germany) can supply 150W and output fiber core/cladding diameter was $200\mu m/240\mu m$. CLSs were fabricated on the fiber having core/cladding/coating diameter as $20\mu m/400\mu m/550\mu m$. CLSs were cooled with a heat sink as shown in the same figure. The power was measured by the detector located in front of the diode laser output.

Attenuation is an important parameter for characterization of CLS. Attenuation can be calculated by using equation 3.16:

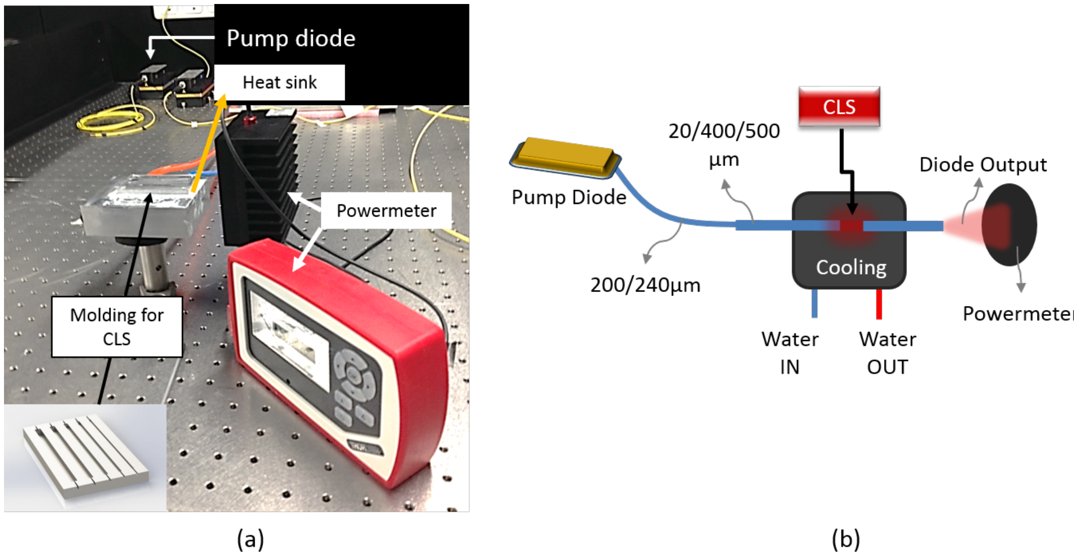

Figure 3.31: Cladding light stripper performance measurement setup.

$$dB_{loss} = -10\log(\frac{P_{output}}{P_{launched}}) \tag{3.16}$$

$P_{launched}$ indicates pump diode laser power. Pump diode laser was characterized as launched power before fabricating CLSs. P_{output} indicates power measured after fabricating CLS. Power output decreases due to CLS and attenuation determines the performance of the CLS. Power measurements are represented in the 3.35.a.

3.8.3.1 Rough Cladding Light Strippers

The first technique used was etching the 1^{st} cladding with rough lapping film ($30\mu m$). It is not easy to polish bare fiber since it becomes fragile after coating is removed. Tünnerman *et al.* has shown that 20dB attenuation can be achieved by using rough CLS [63]. The limitation of producing this type of CLS is that polishing weakens the fiber. Thus, we were not able to etch more than $20-30mm$ long-fiber by polishing. In figure 3.32.a, pump light leaks into the etched cladding and extracted from the fiber. Pump light emitting area is illustrated in figure 3.32.b and reprsented with IR-viewer image in figure 3.32.c. $4dB$ attenuation was achieved with $20mm$-long CLS as shown in figure 3.35.b.

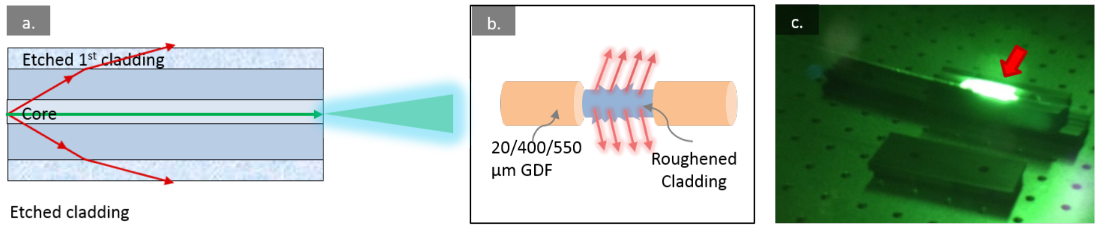

Figure 3.32: (a) Working principle of rough CLS, (b) schematic, (c) IR viewer image of rough CLS.

3.8.3.2 Rough and High Index Poymer Coated Cladding Light Strippers

In the second technique, etched bare fiber mentioned in section 3.8.3.1 was coated with HIP having refractive index 1.539, which makes the CLS structure durable. Also, HIP allows that much more pump light could be removed from the fiber. In figure 3.33.a, pump light exiting from the fiber and in figure 3.33.b, pump light emission scheme are shown. IR-viewer image is represented in figure 3.33.c. $\sim 12dB$ attenuation was achieved as plotted in 3.35.b. Attenuation is increased due to HIP coating comparing to rough-CLS.

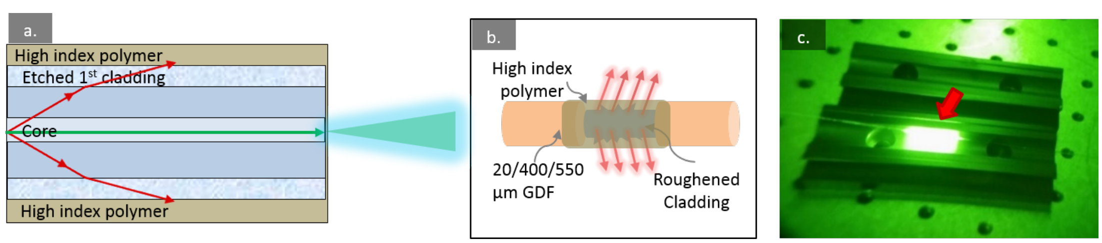

Figure 3.33: (a) Working principle of rough and HIP coated CLS, (b) schematic, (c) IR viewer image.

3.8.3.3 High Index Polymer Coated Cladding Light Strippers

In the this technique high index polymer was coated after 2^{nd} cladding of the fiber was removed. The working principle of HIP-CLS and its representative scheme are shown in figure 3.34.a and b, respectively. In figure 3.34.c, IR-viewer image is represented. The cladding light is emitted through the HIP coated layer.

$\sim 17dB$ attenuation was achieved with $40mm$ long CLS. Sevigny *et al.* found that approximately $17dB$ attenuation with $40mm$ high index polymer with unknown refractive index [66]. The comparison of three types of CLS is represented in figure 3.35.a.

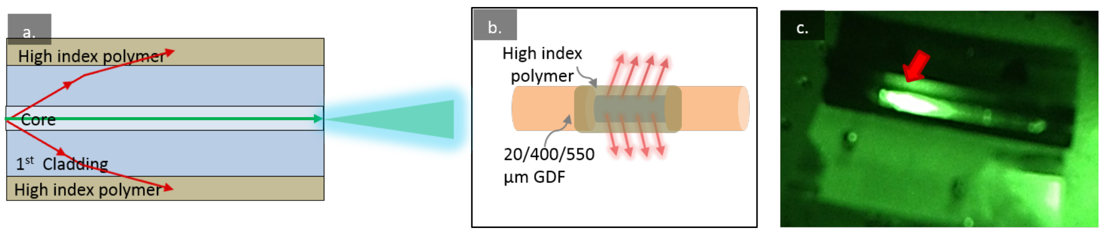

Figure 3.34: (a) Working principle of HIP coated CLS, (b) schematic, (c) IR viewer image.

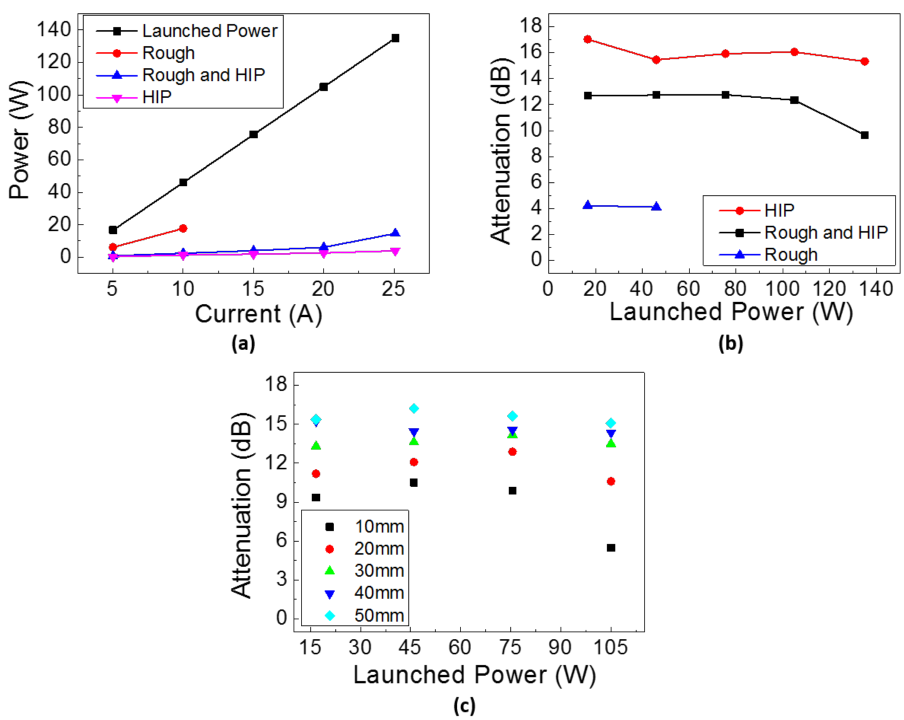

Figure 3.35: (a) Power measurements and (b) attenuation of three types of CLS. (c) Attenuation changing with CLS-length for HIP coated CLS.

The current-power characteristics of the diode laser was obtained without any CLS applied. After rough CLS was applied to the system, the power output decreased. However, the rough CLS was not easy to apply since roughening process made the fiber fragile. Also, thermal management could not be applied since it was a free-space CLS. Thus, the local temperature increase was observed in rough CLS and we were not be able to launch more power. The output power of other types of CLS was very low, meaning that the attenuation due to CLSs were high. Also, the full power of the laser diode could be launched to both rough-HIP coated and HIP coated CLS since the polymer provided a contact between CLS and the heat sink. Thus, the CLSs was able to be cooled with heat sink and the temperature of the CLSs was kept stable. The attenuation values are shown in figure 3.35.b. 4dB, 12dB and 17dB attenuation values were achieved by rough, rough-HIP coated and HIP coated CLSs, respectively. The dependence of attenuation on CLS-length was also investigated by using $10mm$, $20mm$, $30mm$, $40mm$ and $50mm$ HIP coated CLSs. The increase due to CLS length can easily be seen from the figure 3.35.c. Attenuation is increased with the increasing CLS length.

3.8.3.4 Cascaded Cladding Light Strippers

The last technique is quite similar to HIP-CLS case. This CLS structure was suggested by Hou *et al.* that the pump light should be gradually removed in order to obtain homogeneous thermal loading, which occurs more localized in the HIP coating technique [65]. The solution for localized thermal heating is to remove the pump light segment by segment. Figure 3.36 shows those segments which were obtained by removing the low-index coating. Their low-index coating was partially removed along the fiber and they were coated with HIP. There were five segments in total. In the first segment, a quarter of low-index polymer of the fiber was removed as $10mm$ in length. In the next segment, $10mm$ long low-index polymer was remained. In the third segment, half of the $10mm$-long low-index polymer is removed. $10mm$ long low-index polymer remained in the next segment. Finally, $10mm$-long low-index polymer was removed completely. Low-index polymer removal was performed by using PCS-100-(AFL, USA). In figure 3.36, blade numbers are given for each case.

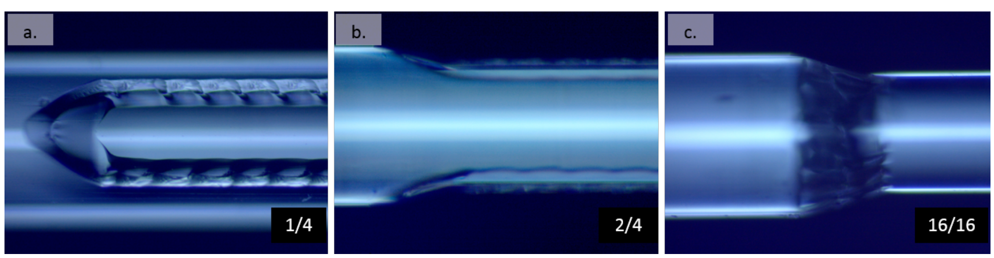

Figure 3.36: Partially coating removed fibers with (a) $\frac{1}{4}$, (b) $\frac{2}{4}$, and (c) $\frac{16}{16}$ steps using PCS-100 (AFL, USA).

All the segments were coated by HIP having refractive index 1.539. The length dependence is also investigated in this study. Attenuation changing with the CLS is shown in figure 3.37.a. Quarter and half stripped segments were kept at the same length as 10mm and the length of the fully stripped segment was altered as 10mm and 20mm. The increase in the attenuation was observed when the length of the fully stripped segment was increased. Cascaded CLS provides a homogeneous heat dissipation due to its segmental structure. Thermal image is represented in figure 3.37.b. Polymer is at $23°C$ when cooled with $19°C$ water. The difference between non-segmental and segmental HIP coated CLS is clearly seen in figures 3.34.c and 3.37.c, respectively. Thermal loading for cascaded CLS is more homogeneous than that for the non-segmental HIP coated CLS. In the inset of figure 3.37, molding which is filled with HIP is represented.

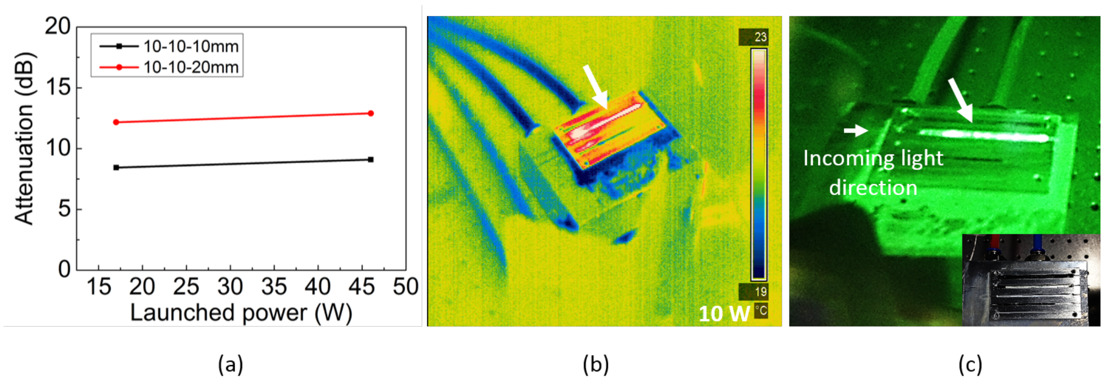

Figure 3.37: (a) Attenuation, (b) IR-viewer image and (c) thermal image at 10W-launched power of Cascaded CLS.

Chapter 4

Fiber Optic Probes in Medical Laser Applications

4.1 Endovenous Laser Ablation (EVLA)

Veneous insufficiency in the lower-extremity is a widespread medical situation, in fact 25% of women and 15% of men suffer from this disease in the USA [67]. The varicose veins are affected or worsened by some conditions, such as pregnancy, aging, standing and sitting for a long time [68]. The primary symptoms cannot be noticed easily by patients, thus, the disease may progress and cause worse symptoms such as night cramps, pain and fatigue [69]. If the varicose vein is not treated before progression, approximately 50% of patients may ultimately suffer from chronic venous insufficiency [70]. The most probable cause of distinctive varicose vein is great saphenous vein (GSV) reflux and even stripping and surgical ligation has been the most certain solution, it causes perioperative morbidity [71]. Since it is identified that the main reason of the varicose vein is the GSV reflux, eliminating of GSV should be the solution [72]. As an alternative to surgical operation, the laser energy was firstly used in an endoluminal operation by Boné in 1999 [73]. This study opened a door for varicose vein treatment, and a procedure had been developed for treatment of GSV by using 810nm laser diode

[74]. The delivery of laser energy into blood vessel lumen has been approved by US Food and Drug Administration in 2002 [75]. There are also other options for treatment of GSV reflux, such as, surgery and RF-ablation. Endovenous laser ablation seems to provide important benefits that are avoidance of general anesthesia and lower rates of complication [76].

Figure 4.1: (a) EVLA operation (adapted from: [77]), (b) ablation procedure (adapted from: [78]).

In figure 4.1.a, a demonstration of EVLA opreration is shown. The fiber probe pull-back procedure is shown in figure 4.1.b. The catheter is inserted inside GSV (figure 4.1.b.1 and 2), and it is pulled-back with specific parameters (such as time-spending on ablation points, pull-back speed), when laser radiation is on (figure 4.1.b.3 and 4) [79].

4.1.1 Wavelength Selection for EVLA

Semi-conductor laser diodes are available in several wavelengths as 810nm, 980nm, 1064nm, 1320nm and 1470nm which are used in endovenous treatment as mentioned in the literature [80, 81, 82, 83]. In the early studies, energy density based mathematical method is used in EVLA, however, recent studies have shown that wavelength absorption of specific chromophore is the key parameter for EVLA operation [84]. The absorption of two chromophores, hemoglobin and water, for these wavelengths are shown in figure 4.2. 810nm is specific to hemoglobin, 980nm is specific to water, 1064nm is absorbed by both hemoglobin and water. 1320nm is specific to water as energy absorbing chromophore, and it is reported that water-specific laser wavelengths are much more efficient than the hemoglobin-specific ones due to less complications after EVLA operation [85]. 1470nm is specific to water and its absorbance is larger than the other wavelengths. In the literature, it is stated that less complication and pain after EVLA treatment is recorded at the higher wavelengths [86]. It is also reported that pain, which depends on heat-induction due to laser radiation, is less at higher wavelengths [87]. Due to those advantages, EVLA operations are performed by using higher wavelengths. Hence, the optical fiber should be transparent at that wavelength regime in order to transmit laser light with a low loss. For the 300-1200nm regime low-OH fiber and for the 400-2200nm regime high-OH fiber should be used, as shown in the figure 4.3.

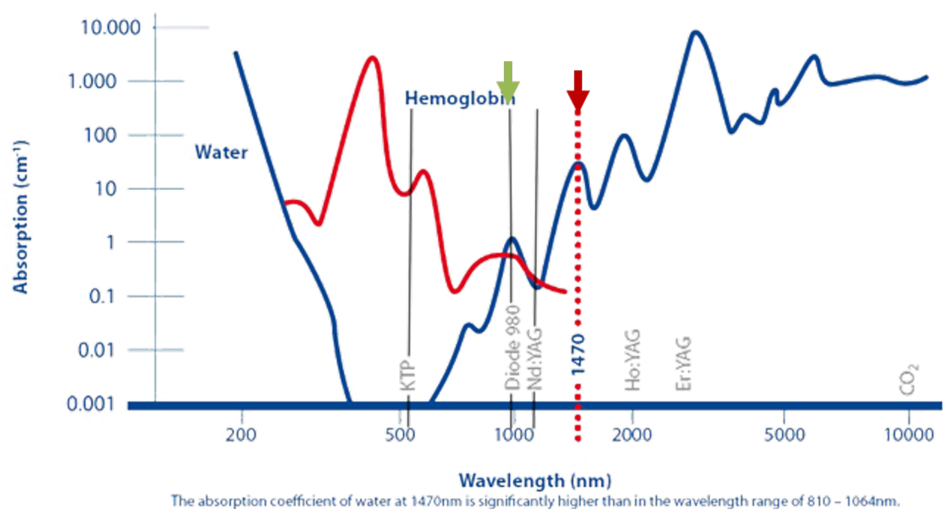

Figure 4.2: Water and hemoglobin absorption graph and laser wavelength preferred for EVLA. (Green arrow indicates 980nm and red arrow indicates 1470nm.) (adapted from: [88])

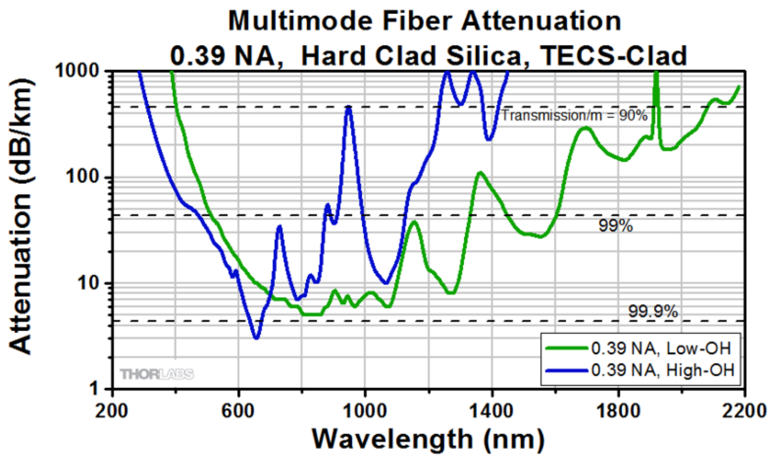

Figure 4.3: Multimode fiber attenuation.(adapted from: [89])

4.2 Test and Measurement of the Medical Laser System

In the market, there are available fiber coupled medical lasers for EVLA such as Osyris-Pharaon (UK-France) and Quanta diode (USA) both of which are operating at 980nm. On the other hand, Leonardo (Germany) is a new product (available since 2014) operating at dual wavelengths at $980 - 1470nm$. In our study, laser system for EVLA application was developed by our research group and E-A Teknoloji Biyomedikal Cihazlar Dijital ve Optik Sistemler Nanoteknoloji Ar-Ge İth. İhr. Taah. San. ve Tic. Ltd. Şti. The laser diode was provided from Lumics, $LU980\_1470D$ (Germany) which is a fiber coupled diode having NA 0.22, SMA connector as output. Moreover, it has 3 individual laser diode emitters: 635nm (pilot laser), 980nm and 1470nm. In figure 4.4, the schematic representation of the laser system is shown. The laser diode is cooled with a feedback system and controlled with an electronic curcuit. Laser works at two operational modes, continuous wave (cw) and pulsed wave (pw) in the order of millisecond for both wavelengths, 980nm and 1470nm. The current supply unit is connected to diode, and provides power to laser diode. A touch screen shows the parameters, namely power, energy density, pulse duration, interval, number of pulses, operation wavelength and duration. Fiber optical probe is the disposable unit of the system. The invasive part of the fiber probe is composed of a fiber tip inside a glass capillary tube which has UV-cured onto the fiber jacket.

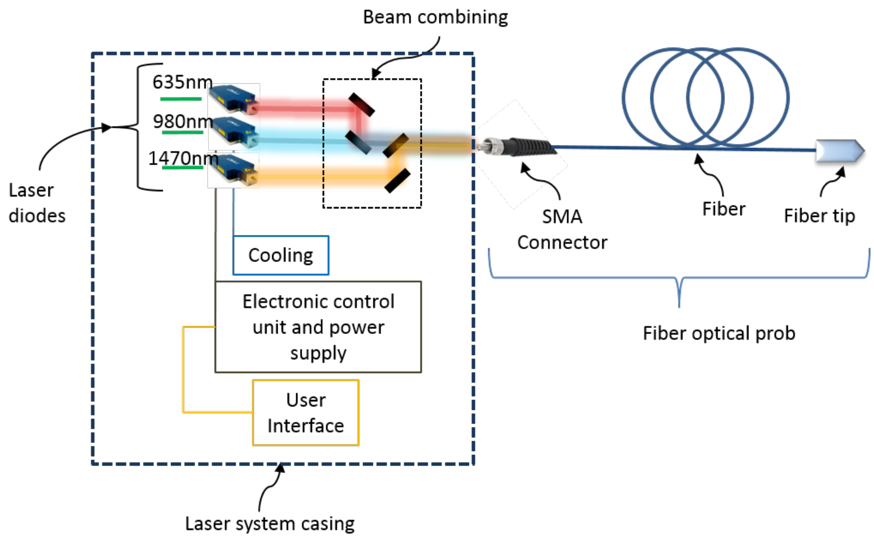

Figure 4.4: Laser system design for EVLA.

4.2.1 Spectral Analysis

In this part, we characterized the diode before building up the medical laser system. The laser diode was investigated in terms of current-voltage characteristics, operational wavelength, shift in the wavelength due to temperature change, current-power characteristics and power stability. The laser diode heats up when operating and this causes a shift in the operating wavelength. In order to form a temperature feedback system, the shift in the wavelength was measured for both $980nm$ and $1470nm$ diodes. The operating power was also monitored as it can change due to an increase in the temperature. To build a stable power supply, the I-V curves were analyzed.

In figure 4.5, characterization of $980nm$ laser diode is shown. The I-V curve is plotted in 4.5.a and the diode current starts to increase linearly when the voltage value of the power supply was $4V$. The spectrum of the $980nm$ laser diode is given in 4.5.b. The wavelength shifted due to cooling temperature is clearly seen. The central wavelength shifted through the higher wavelength values when the cooling

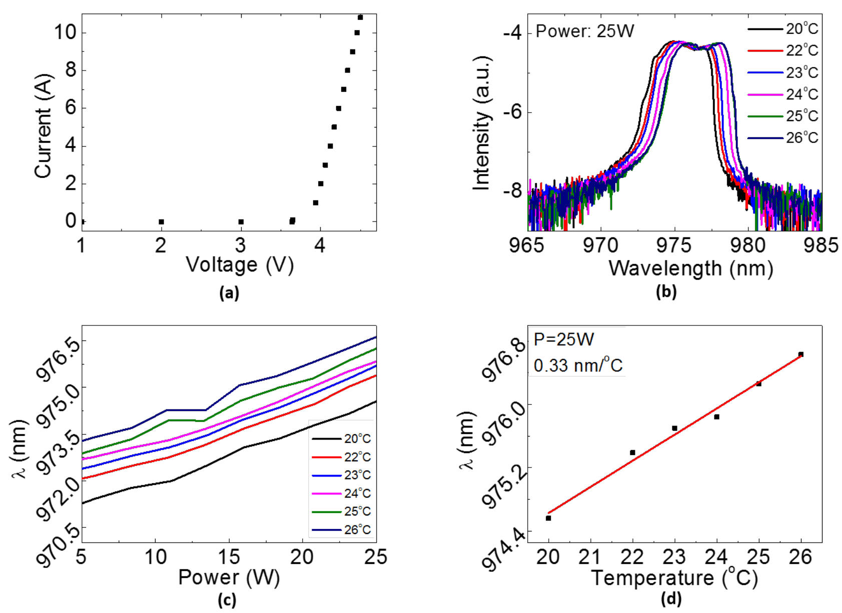

Figure 4.5: Water cooling of 980nm diode. (a) I-V curve for diode. (b) Spectrum between $20-26°C$, (c) wavelength vs. power graph between $20-26°C$, (d) wavelength shift ($0.33\frac{nm}{°C}$) between $20-26°C$.

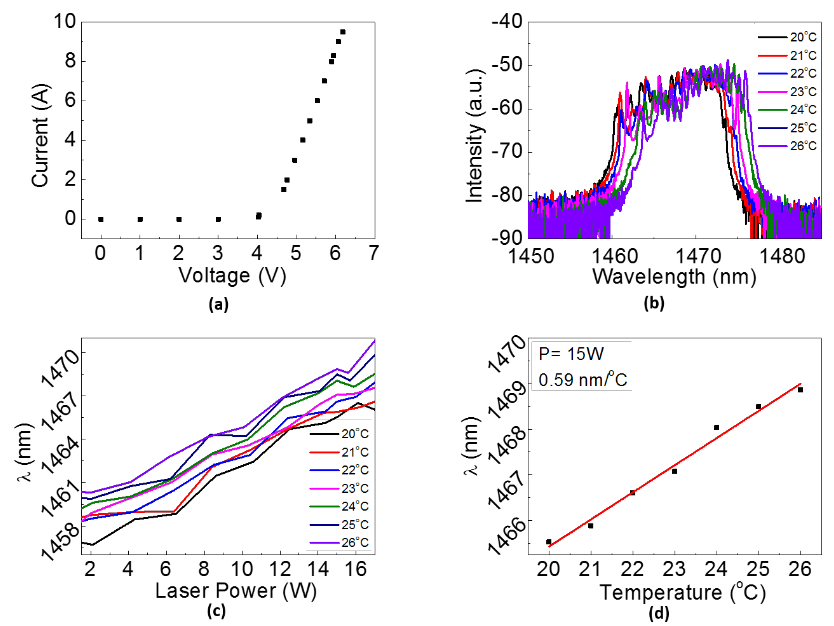

Figure 4.6: Water cooling of 1470nm diode.(a) I-V curve for diode. (b) Spectrum between $20-26°C$, (c) wavelength vs. power graph between $20-26°C$, (d) wavelength shift ($0.59\frac{nm}{°C}$) between $20-26°C$.

temperature increased. The wavelength shift due to power was also investigated and it is represented in figure 4.5.c. The wavelength shifted through the higher wavelengths since the laser diode was heated for the higher power values. In figure 4.6, characterization of the $1470nm$ is represented. I-V curve of the $1470nm$ laser diode is shown in figure 4.6.a and the current started to increase linearly when the voltage value of the power supply was $4.5V$. In figure 4.6.b, the central wavelength shifted through the higher wavelength values due to rising cooling temperature of the water. These characterization graphs served as a roadmap to build our laser system. The diode was cooled with water with different temperatures in order to find the exact temperature range for operation wavelength. Also, the shift in the wavelength due to temperature change was minimized. Depending on these data, a feedback supported cooling system was designed and fabricated. Air-cooling was used to build compact laser system. Supply and electronic units were also fabricated. Finally, all of the units composing the laser system were covered with a case and the medical laser system having a compact and robust design was built. In figure 4.7.a, dual wavelength diode laser characterization setup is shown. The inset image belongs to optical spectrum analyzer (OSA). In figure 4.7.b, medical laser system with feed-back assisted air cooling system and internal power supply is represented.

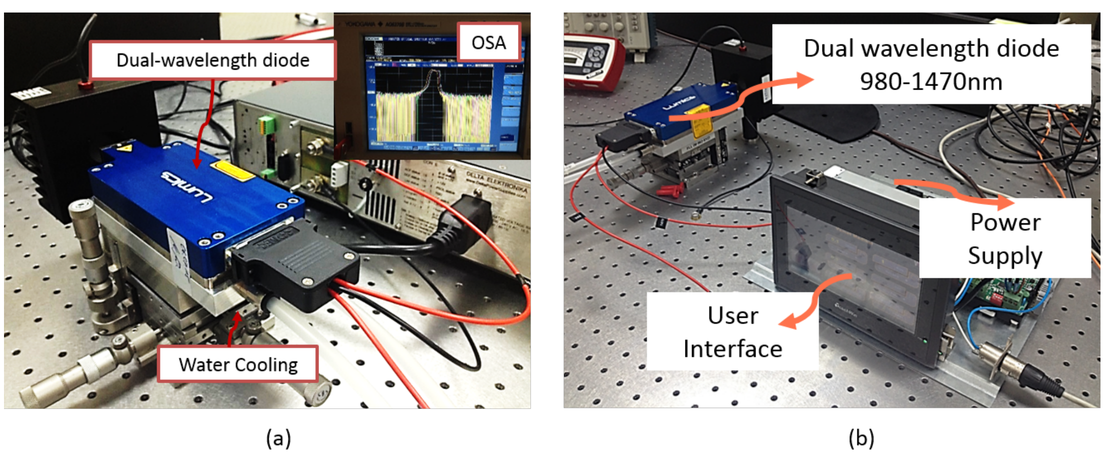

Figure 4.7: (a) Dual wavelength diode characterization setup and inset belongs to optical spectrum analyzer (OSA). (b) Medical laser system with feed-back assisted air cooling system and internal power supply.

Tests and measurements were performed for the fabricated medical laser system. As shown in figure 4.8.a and b, feedback supported cooling system keeps wavelengths stable for both diodes at the wavelength range of EVLA operation as expected. It is also seen that the shift was minimized. In fact, 1470nm diode has almost no wavelength shift since its working power range is less than that of 980nm diode. This means that the heat increase depends on the power increase for both diodes.

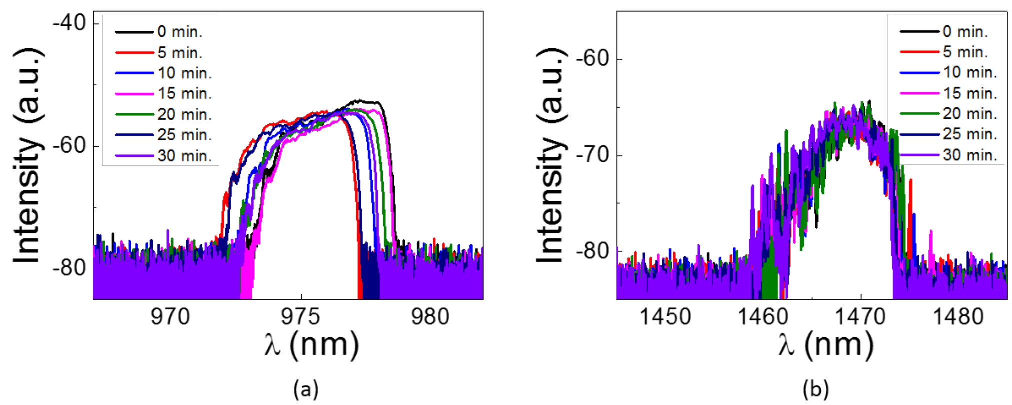

Figure 4.8: Feedback supported air cooling of (a) 980nm and (b)1470nm diode.

4.2.2 Power and Time Domain Analysis

In this section, power measurements and time domain analysis were performed. Power range for 980nm is $0-25W$ and for 1470nm is $0-20W$, as shown in figure 4.9.a. Also, power stability analysis was performed at 25W for 980nm and 15W for 1470nm diodes. These power values are used in EVLA operation, therefore, we tested the stability for that power values. There was almost no change in the power values, meaning that they were stable. The change in the power with time was calculated as $1.6 \times 10^{-4}\frac{W}{s}$ for 980nm diode, and $2.2 \times 10^{-4}\frac{W}{s}$ for 1470nm diode.

As mentioned in section 4.2, the laser system was designed to operate at both cw and pw modes. In figure 4.10, the rise time of the laser pulse is represented

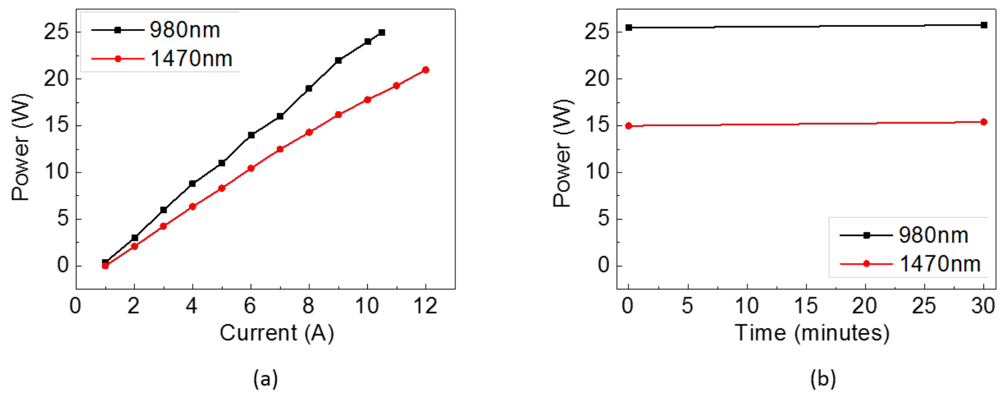

Figure 4.9: (a) I-P graph of the diodes, (b) power stability of the diodes.

which is approximately $4ms$. The parameters, namely duration, interval, number of pulses can be selected from the user interface. These parameters were tested and some of the time domain examples are demonstrated in figure 4.11.a,b and c. The parameters were selected from the user interface and measured with the peak analyzer.

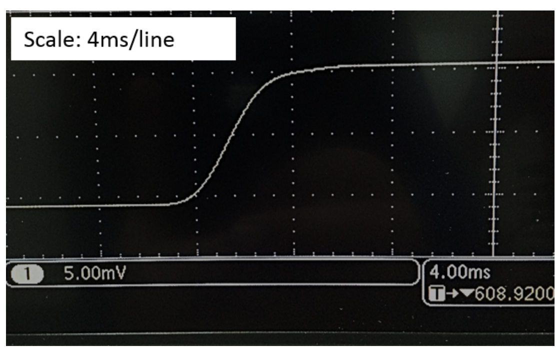

Figure 4.10: Response for $980nm$ and $1470nm$ nm diodes.

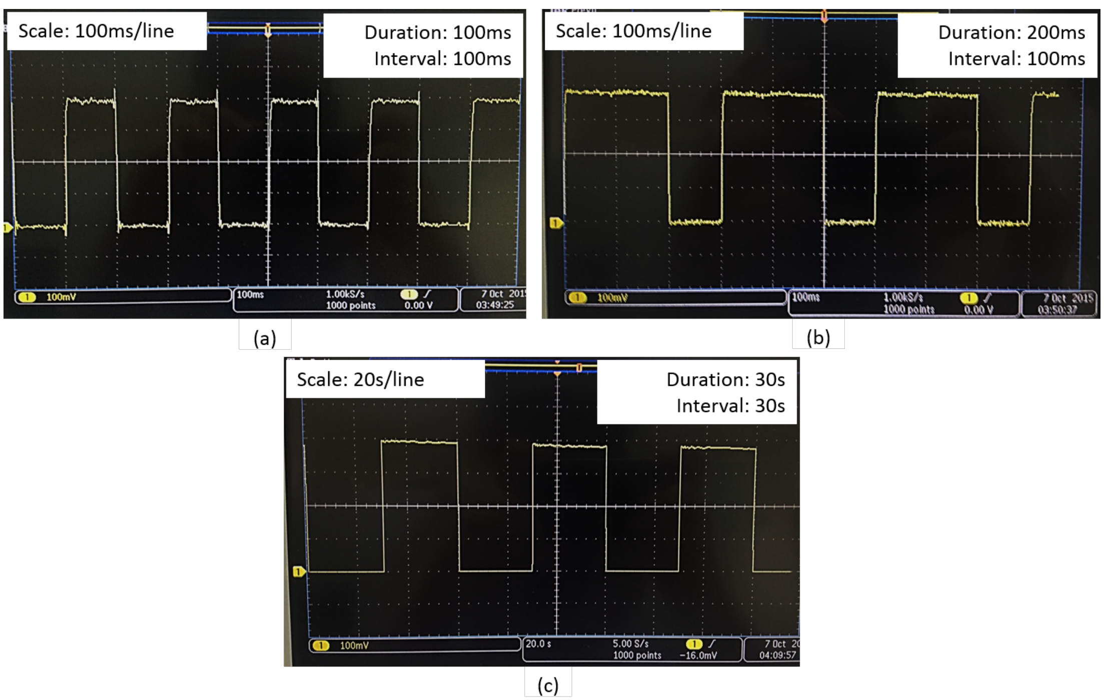

Figure 4.11: Time domain test. (a) 100ms duration, 100ms interval, (b) 200ms duration, 100ms interval, (c) 30s duration, 30s interval.

Chapter 5

Conclusion

The aim of this work was to investigate the application of the fiber optic probes and a dual-wavelength medical laser system. In the fiber optic probe case, flat-ended, side-firing, radial, double radial and diffusing fiber probes were modelled, fabricated and characterized. Our approach was based on manipulation of the fiber tip by polishing. The different fiber tip geometries provide different light emission from the fiber tip. The application of these probes in the medical areas mentioned. The main idea was to control of light deflection by changing the tip geometry and locate the laser radiation onto desired part of the body. In order to fulfil our purpose, the tip geometries were analyzed by ray tracing methods, modelled by Zemax and fabricated by mechanical polishing technique. Their light emission characteristics were represented in intensity distribution versus deflection angle graphs. These graphs clearly shows the spatial distribution of the fiber probes having different geometries. When fabricating a fiber optic probe, the surface roughness is an important parameter in order to eliminate scatering losses originating from rough surface. A new polishing procedure which consists of mechanical and laser polishing was developed in our studies for radial fiber probe. Fine mechanical polishing and CO_2 laser polishing were discussed and demonstrated. Fine-mechanical polishing is labor depended and a time-consuming process especially for radial fiber tips. However, it is very efficient for forming the geometry of the fiber tips. At this point, we showed a different polishing method for radial fiber tips which was performed by CO_2 laser. It is completely labor-independent and it takes less time when comparing to whole mechanical polishing process. We achived $7.87nm$ average roughness after polished at $30\mu m$ lapping film and $3.38nm$ average roughness after polished at $9\mu m$ lapping film.

Two laser applications of two different type of fiber probes were demonstrated. The first one was to use diffusing probe as a cladding light stripper (CLS) in a fiber laser. Since diffusing probes emit light from their cladding surface, they can be used as a CLS. The aim of CLS is to extract unwanted cladding light without disturbing the core light and improve both robustness and beam quality of the fiber laser. Fabricated CLSs were characterized and high attenuation values were achieved. The other laser application of fiber probes was endovenous laser ablation (EVLA). In EVLA operation, laser radition is transmitted through diseased part of the vein, and it is eliminated by heat due to localized laser beam inside the vein. The radial emitting fiber probe was the most suitable one since it emits a ring-shape light.

In the medical laser case, a dual wavelength medical laser was built and characterized. The construction of laser system consisted of three steps. In the first step, dual-wavelength ($980 - 1470nm$) emitting laser diode was characterized. The spectra, shift in the wavelength by changing cooling temperature and I-V curves were determined. In the second step, the feed-back controlled cooling system, electronic unit which controls the power supply and user interface which shows the parameters were fabricated by using the data of first step. In the third part, laser system was covered by a casing and became medical laser system. The final form of medical laser system was also characterized completely.

Bibliography

[1] E. Udd and W. B. Spillman, "Preface," in *Fiber Optic Sensors: An Introduction for Engineers and Scientists*, New Jersey: John Wiley and Sons., 2011.

[2] Y. Matsuura, "Optical fibers for medical application," in *Lasers for Medical Applications: Diagnostics, Therapy and Surgery*, ch. 4, pp. 110–112, Cambridge, UK: Woodhead Publishing, 2013.

[3] M. PERRIN and B. EKLOF, "Randomized controlled trials in the treatment of varicose veins," *Phlebolymphology*, vol. 19(2), 2012.

[4] M. Gurdal, A. Tekin, E. Yucebas, S. Kirecci, and F. Sengor, "Contact neodymium yag laser ablation of recurrent urethral strictures using a side-firing fiber," *Journal of Endourology*, vol. 17(9), 2004.

[5] S. Harries, Z. Amin, and M. Smith, "Interstitial laser photocoagulation as a treatment for breast cancer," *Br J Surg*, vol. 81, 1994.

[6] Skutnik, J. Bolesh, N. Wolfgang, and S. Stefan, "Optical fibers for improved light delivery in photodynamic therapy and diagnosis," 2004.

[7] M. Ishikawa, "Fiber optic connector," Apr. 14 1992. US Patent 5,104,242.

[8] E. Hecht, "Fiber optics," in *Optics* (A. Black, ed.), ch. 5, pp. 193–195, San Francisco, CA, 94111: Addison Wesley, 2002.

[9] J. P. Dakin and R. G. W. Brown, "Optical network arcitectures," in *Handbook of Optoelectronics*, pp. 826–827, NW: CRC, Taylor and Francis, 2006.

[10] J. Crisp and B. Elliot, "Communications," in *Introduction to Fiber Optics*, pp. 6–7, UK: Newnes, 2005.

[11] S. Ozsoy, "Giriş," in *Fiber Optik*, ch. 1, pp. 12–13, İstanbul: Birsen Yayinevi, 2001.

[12] K. Kao and G. Hockham, "Dielectric-fibre surface waveguides for optical frequencies," *IEE PROCEEDINGS*, vol. 133(3), 1966.

[13] F. P. Kapron, D. B. Keck, and R. D. Maurer, "Radiation losses in glass optical waveguides," *Appl. Phys. Lett.*, vol. 17(473), 1970.

[14] K. Thyagarajan and A. Ghatak, "Optical fibers," in *Fiber Optic Essentials* (E. Desurvire, ed.), ch. 4, pp. 28–30, Canada: John Wiley and Sons, 2007.

[15] D. Krohn, T. MacDougall, and A. Mendez, "Preface," in *Fiber Optic Sensors: Fundamentals and Applications, Fourth Edition* (E. Desurvire, ed.), USA: SPIE, 2015.

[16] R. S. Quimby, "Cylindrical waveguides," in *Photonics and Lasers An Introduction*, ch. 4, pp. 43–45, Haboken, New Jersey (simultaneously in Canada): John Wiley and Sons, 2006.

[17] D. Goff, "Principles of operation," in *Fiber Optic Reference Guide*, ch. 3, pp. 21–22, UK: CRC Press, 2002.

[18] R. Tricker, "Critical angle," in *Optoelectronics and Fiber Optic Technology*, ch. 2, pp. 46–47, UK: Newnes, 2002.

[19] M. H. Weik, "Total internal reflection," in *Fiber Optics Standard Dictionary*, pp. 320–321, USA, New York: SPRINGER, 1989.

[20] O. S. of America, "Principles of operation," in *Fiber Optics Handbook: Fiber, Devices, and Systems for Optical Communications*, pp. 1.3–1.7, USA: McGraw-Hill, 2002.

[21] J. Downing, "Reflection," in *Fiber Optic Communications*, pp. 37–39, USA: Thomson, 2005.

[22] K. Thyagarajan and A. Ghatak, "Brewster angle," in *Introduction to Fiber Optics*, printed in USA: Cambridge University Press.

[23] A. Ghatak and K. Thyagarajan, "Propagation characteristics of a step index fiber," in *Introduction to fiber optics*, ch. 9, pp. 173–178, New Delhi: Cambridge University Press, 1997.

[24] J. C. Maxwell, "A dynamical theory of the electromagnetic field," *Phil. Trans. R. Soc. Lond.*, vol. 155, pp. 459–512, 1865.

[25] J. D. Grifths, "Electromagnetics waves in matter," in *Introduction to Electrodynamics*, ch. 9, pp. 382–383, New Jersey: Prentice Hall, 1999.

[26] E. Wikszak, "Bounded modes," in *Inscription of FBG in non-photosensitive and rare-earth doped fibers applying ultrafast lasers*, ch. 2, pp. 70–75, New York: Springer, 2008.

[27] E. Wikszak, *Spatial Distribution*. PhD thesis, Friedrich-Schiller-Universitat JENA, 5 2009.

[28] S. D. Personick, "Optical fibers," in *Fiber Optics: Technology and Applications*, ch. 2, pp. 17–19, New Jersey, USA: SPRINGER, 1985.

[29] O. Ziemann, J. Krauser, P. Zamzow, and W. Daum, "Index profiles and types of fibers," in *Optical Short Range Transmission Sysyems - POF Hand Book*, ch. 2, pp. 70–75, New York: Springer, 2008.

[30] R. S. Quimby, "Losses in optical fibers," in *Photonics and Lasers An Introduction*, ch. 5, pp. 55–57, Haboken, New Jersey (simultaneously in Canada): John Wiley and Sons, 2006.

[31] A. Heinze, W. Beyer, M. Krug, K. Schaarschmidt, R. Sroka, H. G. Stepp, E. Unsoeld, and G. H. Willital, "Modified fiber tips for light application in hollow organs," 1990.

[32] R. Min, N. Khilnani, and S. Zimmet, "Endovenous laser treatment of saphenous vein reflux: Long-term results," *Journal of Vascular and Interventional Radiology*, vol. 14, no. 8, pp. 991–996, 2003.

[33] K. Dowlatshahi, D. Francescatti, and K. J. Bloom, "Laser therapy for small breast cancers," *The American Journal of Surgery*, vol. 184, no. 4, pp. 359–363, 2002.

[34] A. Costello and W. Bowsher, "Laser ablation of the prostate in patients with benign prostatic hypertrophy," *British Journal of Urology*, vol. 69, no. 6, pp. 603–608, 2008.

[35] C. Kittrell, R. M. Cothren, and M. S. Feld, "Laser ablation process and apparatus," 06 1995.

[36] J. OWEN and D. KELLY, "Fiber-optic connector," Oct. 29 2013. US Patent 8,568,039.

[37] J. Hoare, "Minimally invasive therapy.," *Europe PubMed*, vol. 88, no. 6, pp. 19–21, 1992.

[38] "Side-fire fibers for medical technology." http://www.lasercomponents.com/de-en/news/side-fire-fibers-for-medical-technology/. Accessed: 2015-12-28.

[39] "Minimally invasive therapy." http://www.biolitec.com/en/products.htm. Accessed: 2015-12-28.

[40] "Zemax – who we are." http://www.zemax.com/company/about. Accessed: 2015-12-28.

[41] Smith and J. Warren in *Modern Optical Engineering*, p. 436, New York: McGraw-Hill, 2007.

[42] E. F. Robert, T. G. Biljana, and Y. P. R., "Zemax software package, one of the industry's standards," in *Optical System Design*, p. 603, New York: McGraw-Hill, 2008.

[43] J. M. Bennett and R. J. King, "Effect of polishing technique on the roughness and residual surface film on fused quartz optical flats," *Appl. Opt.*, vol. 9, pp. 236–238, 1970.

[44] J. M. Bennett and R. J. King, "Effect of polishing technique on the roughness and residual surface film on fused quartz optical flats," *Appl. Opt.*, vol. 9, pp. 236–238, Jan 1970.

[45] C. Buerhop, B. Blumenthal, and R. Weissmann, "Glass surface treatment with excimer and co2 lasers," *Applied Surface Science*, no. 4, pp. 430–434, 1990.

[46] M. Takahashi and Matsudo, "Polishing apparatus for end faces of optical fibers," 03 1988.

[47] F. Vega, N. Lupon, J. A. Cebrian, and F. Laguarta, "Laser application for optical glass polishing," *Opt. Eng.*, vol. 37(1), 1998.

[48] M. Udrea, H. Orun, and A. Alacakir, "Laser polishing of optical fiber end surface," *Opt. Eng.*, vol. 40(9), 2001.

[49] A. D. McLachlan and F. P. Meyer, "Temperature dependence of the extinction coefficient of fused silica for co2 laser wavelengths," *APPLIED OPTICS*, vol. 26(9), 1987.

[50] C. Buerhop, B. Blumenthal, and R. Weissmann, "Glass surface treatment with excimer and co2 lasers," *Applied Surface Science*, no. 4, pp. 430–434, 1990.

[51] "Minimally invasive laser therapy of venous insufficiency." http://www.biolitec.com/en/applications/phlebology.html. Accessed: 2015-12-29.

[52] "Shaped fiber tip assemblies." https://www.fiberguide.com/product/shaped-fiber-tip-assemblies/. Accessed: 2015-12-29.

[53] "Multimode fiber." https://www.thorlabs.com/thorproduct.cfm? partnumber=FT600EMT. Accessed: 2015-12-29.

[54] T. Watanabe and Y. Matsuura, "Side-firing sealing caps for hollow optical fibers," *Lasers in Surgery and Medicine*, vol. 38, pp. 792–797, 2006.

[55] W. Neuberger and A. Harschack, "Endoluminal laser ablation device and improved method for treating veins," 04 2012.

[56] R. Pashaie, "Single optical fiber probe for fluorescence detection and optogenetic stimulation," *IEEE TRANSACTIONS ON BIOMEDICAL ENGINEERING*, vol. 60, no. 2, pp. 268–280, 2013.

[57] L. Goldman, "Connectors," in *Lasers in Medicine* (R. W. Waynant, ed.), USA: CRC, 2002.

[58] "Cylindrical light diffuser." http://www.medlight.com/. Accessed: 2015-12-29.

[59] A. Galvanauskas, "High power fiber lasers," *Opt. Photon. News*, vol. 15, pp. 42–47, Jul 2004.

[60] A. Wetter, M. Faucher, and B. Sevigny, "High power cladding light strippers," *SPIE*, 2008.

[61] D. J. Richardson, J. Nilsson, and W. A. Clarkson, "High power fiber lasers: Current status and future perspectives," *Opt.Soc. Amer. B, Opt. Phys.*, vol. 27, pp. 63–92, Nov. 2010.

[62] R. Poozesh, "novel method for stripping cladding lights in high power fiber lasers and amplifiers," *J. Lightwave Technol.*, vol. 30, Oct. 2012.

[63] Kliner, A. Hou, Kai-Chung, M. Plötner, C. Hupel, T. Stelzner, T. Schreiber, R. Eberhardt, and A. Tnnermann, "Fabrication and evaluation of a 500 w cladding-light stripper," 2013.

[64] A. Carter, "Damage mechanisms in component s for fiber laser and amplifiers," *Proc. SPIE*, vol. 5647, 2005.

[65] W. Guo, Z. Chen, H. Zhou, J. Li, and J. Hou, "Cascaded cladding light extracting strippers for high power fiber lasers and amplifiers," *IEEE Photonics Journal*, vol. 6, June 2014.

[66] A. Wetter, M. Faucher, and B. Svigny, "High power cladding light strippers," *Proc. of SPIE*, vol. 6873, 2008.

[67] M. Callam, "Epidemiology of varicose veins," *Br J Surg*, vol. 81, pp. 167–173, 1994;.

[68] S. Rose, "Anatomic observations on causes of varicose veins," *St Louis: Quality Medical Publishing*, pp. 12–17, 1999.

[69] W. Fegan, R. Lambe, and M. Henry, "Steroid hormones and varicose veins," *Lancet*, pp. 1070–1071, 1967.

[70] L. Widmer, T. Mall, and H. Martin, "Epidemiology and social medical importance of diseases of the veins.," *Munch Med Wochenschr*, pp. 1139–1142, 1974.

[71] G. McMullin, P. Smith, and J. Scurr, "Objective assessment of high ligation without stripping the long saphenous vein.," *Br J Surg*, pp. 1139–1142, 1991.

[72] P. Stonebridge, N. Chalmers, T. Beggs, A. Bradbury, and C. Ruckley, "Recurrent varicose veins: a varicographic analysis leading to a new practical classification.," *Br J Surg*, pp. 60–62, 1995.

[73] C. Boné, "Endovenous laser: a new minimally invasive method of treatment for varicose veins-preliminary observations using an 810 nm diode laser.," *Dermatol Surg*, pp. 117–122, 2001.

[74] L. Navarro, R. Min, C. Boné, A. Bradbury, and C. Ruckley, "Tratamiento endoluminal delas varices con laser de diodo: estudio preliminary.," *Rev Patol Vasc*, pp. 35–46, 1999.

[75] C. V. et al., "Iatrogenic complications following laser ablation of varicose veins," *Vascular Surgery, InTech*, pp. 151–164, 2012.

[76] J. I. ALMEIDA, "Rfa versus laser ablation of the saphenous vein," *SUPPLEMENT TO ENDOVASCULAR*, pp. 15–19, 2014.

[77] "Vein procedures." http://scarlessveincare.com/procedures/. Accessed: 2015-12-28.

[78] "Endovenous laser ablation." http://www.ambradsurgery.com/endovenous-laser-ablation/. Accessed: 2015-12-28.

[79] R. J. Min, N. Khilnani, and S. E. Zimmet, "Endovenous laser treatment of saphenous vein reflux: Long-term results," *J Vasc Interv Radiol*, pp. 991–996, 2003.

[80] V. den R Bos, L. Arends, M. Kockaert, M. Neumann, and T. Nijsten, "Endovenous therapies of lower extremity varicosities: a metaanalysis.," *J Vasc Surg*, vol. 49(1), pp. 230–9, 2009.

[81] H. S. Kim, I. J. Nwankwo, K. Hong, and P. S. McElgunn, "Lower energy endovenous laser ablation of the great saphenous vein with 980 nm diode laser in continuous mode," *Cardiovasc Intervent Radiol*, vol. 29, pp. 64–69, 2006.

[82] F. Pannier, E. Rabe, and U. Maurins, "First results with a new 1470-nm diode laser for endovenous ablation of incompetent saphenous veins," *Phlebology*, vol. 24, pp. 26–30, 2009.

[83] L. S. Kabnick, "Outcome of different endovenous laser wavelengths for great saphenous vein ablation," *J Vasc Surg*, vol. 43, pp. 88–93, 2006.

[84] E. Prince, S. Ahn, G. Dubel, and G. Soares, "An investigation of the relationship between energy density and endovenous laser ablation success: does energy density matter?," *J Vasc Interv Radiol.*, vol. 19(10), pp. 1449–1453, 2008.

[85] S. Herdemann, "Endovenous treatment of the great saphenous vein using a1,320 nm nd:yag laser causes fewer side effects than using a 940 nm diode laser.," *Dermatol Surg.*, vol. 31(12), pp. 1678–1683, 2005.

[86] L. Kabnick, "Outcome of different endovenous laser wavelengths for great saphenous vein ablation.," *J Vasc Surg.*, vol. 43(1), pp. 88–93, 2006.

[87] R. Jeffrey, "Saphenous laser ablation at 1470nm targets the vein wall, not blood," *Vascular and Endovascular Surgery*, vol. 43(5), pp. 467–472, 2009.

[88] "Water absorption." http://www.gigaalaser.com/images/waterabsorption.png. Accessed: 2016-01-02.

[89] "Multimode fiber attenuation." http://www.thorlabs.de/images/TabImages/HardCladSilica039 TECSLarge850.gif. Accessed: 2015-12-29.